Multi-phonon (percolation) behavior and local clustering of CdxZn1–xSe-cubic mixed crystals (x ≤ 0.3): A Raman–ab initio study

Mohamad Baker Shoker, Olivier Pagès, H. Dicko, V. J B Torres, Andrei V. Postnikov, A. Polian, F. Firszt, K. Strzalkowski, Aotmane En Naciri, Laurent Broch, et al.

To cite this version:

Mohamad Baker Shoker, Olivier Pagès, H. Dicko, V. J B Torres, Andrei V. Postnikov, et al.. Multi-phonon (percolation) behavior and local clustering of CdxZn1–xSe-cubic mixed crystals (x ≤ 0.3): A Raman–ab initio study. Journal of Applied Physics, 2019, 126 (10), pp.105707. 10.1063/1.5111106 . hal-02289768

HAL Id: hal-02289768
https://hal.univ-lorraine.fr/hal-02289768v1

Submitted on 17 Sep 2019

Journal of
Applied Physics

Multi-phonon (percolation) behavior and local clustering of $Cd_xZn_{1-x}Se$-cubic mixed crystals ($x \leq 0.3$): A Raman–*ab initio* study

Cite as: J. Appl. Phys. **126**, 105707 (2019); https://doi.org/10.1063/1.5111106
Submitted: 23 May 2019 . Accepted: 25 July 2019 . Published Online: 12 September 2019

M. B. Shoker, O. Pagès, H. Dicko, V. J. B. Torres, A. V. Postnikov, A. Polian, F. Firszt, K. Strzałkowski, A. En Naciri, L. Broch, M. N. Rao, R. Rao, A. Maillard, and J.-P. Itié

View Online Export Citation CrossMark

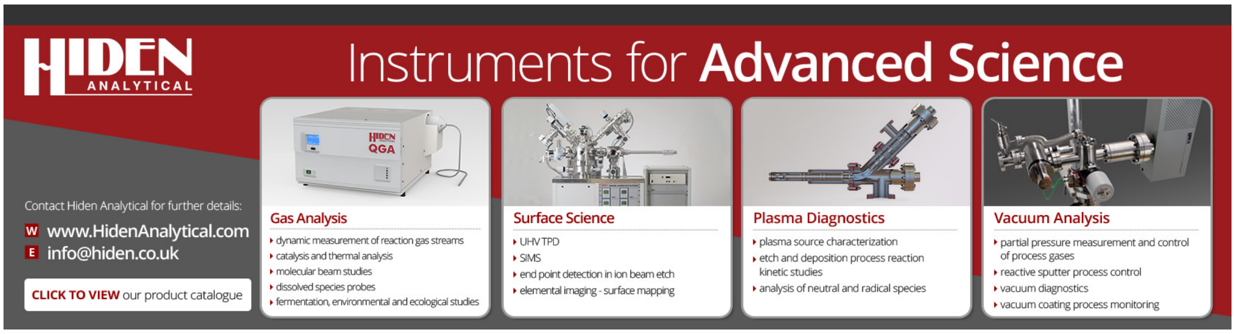

AIP Publishing

Journal of Applied Physics ARTICLE scitation.org/journal/jap

Multi-phonon (percolation) behavior and local clustering of $Cd_xZn_{1-x}Se$-cubic mixed crystals ($x \leq 0.3$): A Raman–*ab initio* study

Cite as: J. Appl. Phys. **126**, 105707 (2019); doi: 10.1063/1.5111106
Submitted: 23 May 2019 · Accepted: 25 July 2019 ·
Published Online: 12 September 2019

M. B. Shoker,[1] O. Pagès,[1,a)] H. Dicko,[1] V. J. B. Torres,[2] A. V. Postnikov,[1] A. Polian,[3] F. Firszt,[4] K. Strzałkowski,[4] A. En Naciri,[1] L. Broch,[1] M. N. Rao,[5] R. Rao,[5] A. Maillard,[6] and J.-P. Itié[7]

AFFILIATIONS

[1] LCP-A2MC, Institut Jean Barriol, Université de Lorraine, Metz F-57078, France
[2] Departamento de Fisica and I3N, Universidade de Aveiro, 3810-193 Aveiro, Portugal
[3] Institut de Minéralogie, de Physique des Matériaux et de Cosmochimie, Sorbonne Université—UMR CNRS 7590, F-75005 Paris, France
[4] Institute of Physics, Nicolaus Copernicus University, 87-100 Toruń, Poland
[5] Solid State Physics Division, Bhabha Atomic Research Centre, Mumbai 400085, India
[6] LMOPS, Institut Jean Lamour, Sup'Elec, Université de Lorraine, Metz F-57078, France
[7] Synchrotron SOLEIL, L'Orme des Merisiers Saint-Aubin, BP 48, F-91192 Gif-sur-Yvette Cedex, France

Note: This paper is part of the Special Topic on Highly Mismatched Semiconductors Alloys: from Atoms to Devices.

[a)] **Author to whom correspondence should be addressed:** olivier.pages@univ-lorraine.fr

ABSTRACT

We present a polarization-dependent pure transverse-optic (TO) Raman study of high-quality $Cd_xZn_{1-x}Se$ single crystals with zincblende (cubic) structures ($x \leq 0.3$) covering both the phonon and phonon-polariton variants of the TO modes, using suitable backward and near-forward scattering geometries, respectively. Insight into the native phonon regime of the phonon-polaritons is obtained at intermediate composition of the random crystal ($x = 0.5,\ 0.3$) and at the (Cd,Zn)-dilute limits ($x \sim 0.1$; using prototype impurity motifs) by applying *ab initio* codes to large supercells (64–216 atoms), with special attention to both the Raman intensities and the phonon frequencies. The experimental (Raman) and theoretical (*ab initio*) results converge onto a percolation-type three-phonon [1 × (Cd-Se), 2 × (Zn-Se)] pattern for $Cd_xZn_{1-x}Se$. On the practical side, the interplay between the oscillator strengths of the two Zn-Se Raman modes is used to diagnose a pronounced trend toward local clustering in the studied crystals, presumably an early sign of the composition-induced zincblende ↔ wurtzite structural transition ($x \sim 0.3$). The deviation from the ideal Zn ↔ Cd random substitution is estimated by working out a zincblende-version of the percolation model equipped with a relevant order parameter κ. The model is based on a sensitivity of the Zn-Se vibration to its local environment at the second-neighbor scale, independently supported by *ab initio* calculation of the Raman spectra in their dependence on κ (adjusted by simulated annealing).

I. INTRODUCTION

The $Cd_xZn_{1-x}Se$ semiconductor mixed crystal exhibits a direct optical gap that can be tuned throughout the visible spectrum by finely adjusting the composition x.[1–4] For this reason, $Cd_xZn_{1-x}Se$ enters as a key component in many optoelectronic devices.[5–7] As is well known, the electron-phonon scattering processes adversely affect the optical and transport properties of electrons in semiconductors.[8–10] Therefore, when dealing with such a complex semiconductor system as a mixed crystal, it is of prime importance to elucidate the nature of its phonon-mode behavior. This is still an open issue in the case of $Cd_xZn_{1-x}Se$, as detailed below.

The vibrational properties of $Cd_xZn_{1-x}Se$ are interesting on the fundamental side due to the unusually large contrast in the structural properties of its parent compounds. The lattice mismatch $\left(\frac{\Delta a}{a} \sim 7\%\right)$ of $Cd_xZn_{1-x}Se$ is comparable to that achieved with the most contrasted $In_{1-x}Ga_x$-based $\left(\frac{\Delta a}{a} \sim 7\%\right)$ and $Zn_{1-x}Be_x$-based $\left(\frac{\Delta a}{a} \sim 9\%\right)$ III-V and II-VI mixed crystals.[11] Moreover, unlike the latter, its parent systems adopt different crystal structures at ambient conditions, the cubic zincblende for ZnSe and the hexagonal wurtzite for CdSe.[3,12] The single crystals keep the ZnSe-like zincblende structure up to moderate Cd content ($x \leq 0.3$).[13] The zincblende and wurtzite structures coexist at intermediate composition ($0.3 \leq x \leq 0.5$), and the crystal structure turns pure wurtzite above $x = 0.5$.[3,12] In contrast, epitaxial layers can be grown with zincblende structures throughout the entire composition domain using appropriate (GaAs or InP) substrates.[3,5,7] Altogether, the contrasts in bond length and crystal structures are expected to generate dramatic bond distortions at the local scale in $Cd_xZn_{1-x}Se$, with concomitant impact on the vibrational properties. This is especially true near the composition-induced structural transition ($x \sim 0.3$).

The phonon properties are conveniently studied at the laboratory scale by using Raman scattering or far-infrared reflectivity (IR). Due to the quasivertical dispersion of light, these optical techniques operate near Γ ($q = 0$), i.e., within the first few percent of the Brillouin zone. At this limit, only the optic modes propagate. In the case of $Cd_xZn_{1-x}Se$, the optic modes refer to transverse (TO) and longitudinal (LO) displacement of the quasirigid ($q \sim 0$) Se-anion sublattice against the Cd/Zn-cation sublattice, which cations vibrate in phase but with different magnitudes. Though the Raman/IR insight is restricted to Γ, the spectral resolution is high, i.e., much better (by roughly one order of magnitude) than that achieved by inelastic neutron scattering[14] or by inelastic X-ray scattering[15]—with counterpart an access to the phonon dispersion throughout the Brillouin zone. Raman scattering and IR-reflectivity are thus techniques of choice to address the nature of the phonon-mode behavior of a mixed crystal.

The Raman and IR spectra of $Cd_xZn_{1-x}Se$ are well documented. The corpus of data is large, initiated back to the 1970s. By way of highlights of the $Cd_xZn_{1-x}Se$ Raman/IR studies, we retain several contributions detailed below. It should be mentioned that, generally, the quality of the Raman/IR signal degrades by increasing the Cd content.[16,17] Considering more specifically single crystals, the degradation occurs by crossing the zincblende → wurtzite structural transition ($x \sim 0.3$).[18]

In his pioneering Raman study of $Cd_xZn_{1-x}Se$ single crystals and polycrystals spanning the composition domain, Brafman[19] excludes the TO modes from the discussion due to their complexity. At the term of his careful LO analysis, he concludes about a one-mode behavior for $Cd_xZn_{1-x}Se$, corresponding to an unique (Zn-Se,Cd-Se)-mixed LO mode that shifts smoothly between the parent frequencies with a stable Raman intensity when x changes. Such behavior is commonly grasped by the modified-random-element-isodisplacement (MREI) model in its most compact version.[20]

Valakh *et al.* pursued the Raman study using monocrystals ($x \leq 0.6$) and tackled the TO modes, while generally subscribing to Brafman's view of a basic one-mode behavior for $Cd_xZn_{1-x}Se$.[21,22] A problem arose herewith that the TO feature exhibits a clear bimodal pattern at any alloy composition, with a significant contribution outside the main TO–LO band. Through a series of detailed Raman studies, the cited authors developed a view that the presumed unique zone-center TO mode acquired a fine structure due to a Fano interference with a two-phonon acoustic continuum (2A) from the Brillouin zone-edge. The discussion was supported by a careful contour modeling of the Fano-distorted Raman lineshape.[23] The Fano-coupling was further tested experimentally by extending the Raman study to low (nitrogenlike) temperatures, at which the two-phonon Raman continuum is expected to collapse (much more rapidly than the one-phonon zone-center TO signal). Contrary to expectations, the bimodal TO pattern survived at low temperatures, being even better resolved than at high temperatures (450 K).[23] In our view, such anomaly reveals that the bimodal TO pattern is not directly due to the Fano interference (even if the latter may subsequently enhance it)—in any case clearly evidenced by Valakh *et al.*—but is intrinsic to $Cd_xZn_{1-x}Se$-alloying. This observation definitely rules out the one-mode behavior for $Cd_xZn_{1-x}Se$. Valakh *et al.* further identified an additional minor mode within the main TO–LO band, which they assigned as an impurity mode.[23] Effectively, this leads to a conclusion about an overall three-mode behavior in total for $Cd_xZn_{1-x}Se$, even if the authors did not put it that way.

Alonso *et al.*[24] assigned the minor in-band mode in terms of an impurity mode with (Zn-Se, Cd-Se)-mixed character. This assignment was lately adopted also by Avendaño-López *et al.*[25] It is supported by a MREI description based on identification of the ZnSe:Cd ($x \sim 0$) and CdSe:Zn ($x \sim 1$) impurity modes at higher frequencies than the parent TO_{ZnSe} and TO_{CdSe} modes. The frequencies of the main LO Raman modes measured with a series of zincblende-type epitaxial layers covering the whole composition domain were successfully modeled on this basis. However, the assignment of the impurity modes remains doubtful, in that the used MREI description produces a second-neighbor Cd ↔ Zn force constant larger than the first-neighbor Cd ↔ Se and Zn ↔ Se ones. This is not realistic physically, as noted by the cited authors.[24]

A decisive step in the understanding of the phonon-mode behavior of $Cd_xZn_{1-x}Se$ was taken by shifting from Raman scattering to IR-reflectivity, especially when applying the latter to single crystals. This was done through a series of studies,[26–28] lately concluded by Kozyrev.[13,18,29] As IR-reflectivity detects the TO–LO absorption bands, it treats the TO and LO modes on equal footing. As such, it conveniently offers a complete and consistent overview of the optic modes of a mixed crystal in a single shot. An additional advantage when using single crystals is that the relative dielectric function $\varepsilon_r(\omega, x)$ of the system can be reconstructed numerically by the Kramers-Krönig transformation of the raw IR-reflectivity data, with no need of modeling. A subsequent insight into the TO- and LO-like Raman signals is then achieved by calculating $\mathrm{Im}\{\varepsilon_r(\omega, x)\}$ and $\mathrm{Im}\{-\varepsilon_r(\omega, x)^{-1}\}$, which capture the resonances behind the dispersions of the TO $\left[\varepsilon_r(\omega, x) = \frac{q^2\omega^2}{c^2}\right]$ and LO $[\varepsilon_r(\omega, x) = 0]$ modes, respectively.

The bimodal pattern behind the main TO feature earlier detected by Valakh *et al.*[21–23] was unambiguously evidenced by IR-reflectivity. As apparent in the abundant IR data reported by Kozyrev spanning large-to-dilute Cd contents ($x = 0.80 - 0.08$, see Fig. 1 of Ref. 18), the lower submode of the fine structure strengthens at the expense of the upper one when the Cd content increases.

This suggests that the latter features relate to Cd-Se and Zn-Se, respectively. The stable frequency gap between the two submodes (~15 cm^{-1}) leads to a prediction that the lower CdSe-like submode should weaken toward the ZnSe:Cd ($x \sim 0$) impurity mode below the $TO_{\rm ZnSe}$ parent mode, and not above it, as earlier proposed by Alonso *et al.*[24] and by Avendaño-López *et al.*[25] In fact, by using the Green's function method, Kozyrev predicted that the ZnSe:Cd ($x \sim 0$) impurity mode should emerge as a gap mode between the acoustic and optic bands of the phonon density of states of the host ZnSe matrix, i.e., at ~182 cm^{-1}.[18] Such feature was actually detected by IR reflectivity. The re-assignment of the ZnSe:Cd ($x \sim 0$) mode below the parent $TO_{\rm ZnSe}$ mode, supported by the IR data, contradicts an assignment of the minor in-band mode as an impurity one by Alonso *et al.*[24] and by Avendaño-López *et al*,[25] offering for the moment no alternative explanation.

By analogy with ZnSe$_{1-x}$Te$_x$,[30] that was for long taken as representative for the one-mode behavior (innovative insight has been gained recently by applying temperature-dependent extended X-ray absorption fine structure measurements[31] to ZnSe$_{1-x}$Te$_x$—Ref. 32)—as Cd$_x$Zn$_{1-x}$Se,[33,34] Kozyrev has recently discussed the TO fine structure in terms of a three-mode [1 × (Cd-Se), 2 × (Zn-Se)] percolation-type pattern.[29] An overview is given in Fig. 1. In this description, the lower mode refers to Cd-Se vibrations, while the Zn-Se doublet distinguishes between Zn-Se vibrations in the ZnSe-like (main/central feature) and CdSe-like (upper/minor in-band feature) environments, respectively. However, a quantitative insight is needed either to secure or to rule out the percolation picture for Cd$_x$Zn$_{1-x}$Se. This is the motivation for the current study.

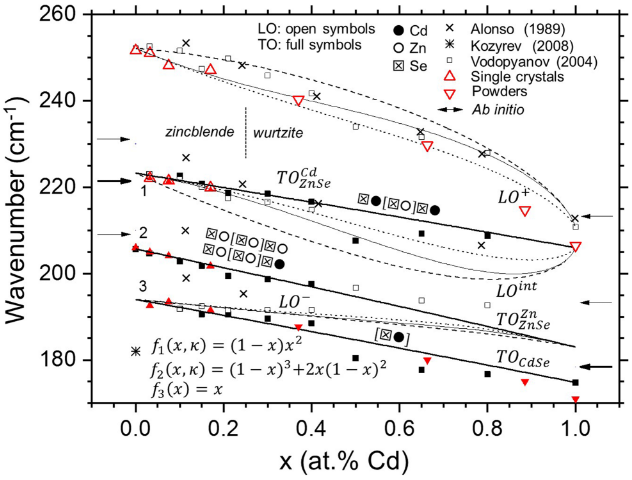

FIG. 1. Cd$_x$Zn$_{1-x}$Se TO and LO modes. TO (full symbols) and LO (open symbols) IR-reflectivity data from single crystals (squares, Ref. 28) and Raman data from thin films (crosses, Ref. 24) compared to present (triangles) TO and LO Raman data. The TO branches are taken linear in the zincblende domain (thick lines). Arrows at the ends: present *ab initio* results (see Fig. 4). Star: Green's function calculation (Ref. 18). *f*-terms: fractions of 1D-oscillators behind the TO modes, defined at the second-neighbor scale in the case of a random Zn ↔ Cd substitution. Corresponding predictions for the LO frequencies are reported in the random ($\kappa = 0$, thin lines) and clustered ($\kappa = 0.5$, dotted lines) cases and also for a sensitivity of the Zn-Se vibration at the first-neighbor scale in the random case (dashed lines). Thick/thin arrows refer to *ab initio* parent/impurity modes (taken from Fig. 4).

Entering more details, it is remarkable that the upper/in-band TO mode hardly shows up in the Raman/IR spectra. Besides, as apparent in Fig. 1, whereas the TO–LO splitting is large for the central/dominant mode (comparable to that observed in each parent compound), it is small for the lower mode (hardly exceeding a few cm^{-1}) and just negligible for the upper/minor in-band one. The latter mode is even characterized by a slight LO–TO inversion.[28] This aspect, in particular, has attracted considerable attention in the literature: not so much the inversion per se, but its surprisingly small magnitude. The two-mode versions of the modified random element isodisplacement (MREI) model used by Alonso *et al.*[24] and by Avendaño-López *et al.*[25] (checked by us, not shown) as well as the ZnSe$_{1-x}$Te$_x$-like three-mode version of our own percolation model advanced by Kozyrev[29] (see below) consistently mimic the LO–TO inversion for the in-band mode, albeit with a much larger magnitude than that observed experimentally. The two-mode model of Jahne[35,36] operated by Vinogradov *et al.*[27] considers an impurity mode (due to the anti-phase vibration of the Cd- and Zn-cationic sublattices against the stable Se anions in between) on top of a lattice mode (due to the vibration of the common Cd/Zn-cationic sublattice against the Se-anionic one). This model is likewise satisfactory on the main trends (omitting that a two-mode description necessarily fails to account for an overall three-mode pattern) and more consistent than the MREI model with the experimental findings regarding the magnitude of the LO–TO inversion of the in-band mode. However, again, the theoretical inversion overestimates the experimental one. Besides, all the cited models predict a significant TO-intensity for the in-band Raman mode throughout the composition domain (an outline is given in the course of the discussion), in contradiction with the experimental findings. An additional disconcerting feature revealed by Kozyrev is that the oscillator strength awarded to the in-band mode—which directly governs the magnitude of its LO–TO inversion and its TO Raman intensity as well—is roughly three times larger for Cd$_x$Zn$_{1-x}$Se epitaxial layers than for single crystals (see Fig. 2 of Ref. 29). The origin for such discrepancy remains unexplained so far. We retain that the amount of oscillator strength awarded to the minor/in-band mode is sensitive to the growth conditions and thus is not an intrinsic quantity.

Our ambition in this work is to contribute to the understanding of the phonon-mode behavior of Cd$_x$Zn$_{1-x}$Se by performing a pure-TO Raman study of pure zincblende (noted Cd$_x$Zn$_{1-x}$Se-c, the suffix stands for "cubic") single crystals ($x \leq 0.3$) corresponding to a high-quality Raman signal, combining experiment and theory. Both the phonon-polariton (PP) regime—that remains unexplored with Cd$_x$Zn$_{1-x}$Se—and the native purely-mechanical TO regime of the PP modes are addressed using suitable near-forward (transmissionlike) and backward (reflectionlike) scattering geometries, respectively. The latter regime, in particular, is interesting because the purely-mechanical TO modes (abbreviated TO from now on) do hardly couple (in contrast with the polar LO[37] and PP[38] ones). As such, they preserve the natural richness of the phonon pattern of such a complex system as a mixed crystal. This is the *sine qua non* condition to achieve its refined understanding.

Independent insights into the Raman frequencies and Raman intensities of the multi-TO modes are gained via *ab initio* calculations of the Γ-projected phonon density of states (Γ-PhDOS) and of the actual Raman spectrum. Such *ab initio* insights are obtained by applying the Siesta[39] and AIMPRO[40–42] codes to large (up to ∼200 atoms) zincblende supercells at both ends of the composition domain ($x \sim 0.1$) and at intermediary composition ($x \sim 0.5$), respectively. They are required in the first place to check *de visu* the assignment of the three $Cd_xZn_{1-x}Se$-c TO modes, i.e., via a direct examination of the vibration patterns due to prototype impurity motifs ($x \sim 0.1$; Siesta). They are further needed to discuss the abnormally weak Raman intensity of the upper in-band mode at intermediary composition ($x \sim 0.5$ and 0.3; AIMPRO), which presumably relates to its minimal LO–TO inversion (as explained above).

II. SAMPLES, EXPERIMENT, AND *AB INITIO* CALCULATIONS

A. $Cd_xZn_{1-x}Se$ mixed crystals: Structural and optical properties

We dispose of a series of large (cylinders, 5–10 mm in length, ∼8 mm in diameter) high-quality $Cd_xZn_{1-x}Se$ single crystals with well-spanned compositions throughout the composition domain ($x = 0$, 0.032, 0.075, 0.170, 0.370, 0.665, 0.885). They were grown from the melt under equilibrium conditions using the high-pressure Bridgman method.[43] The starting materials are mixtures of ZnSe and CdSe powders, each with purity 5*N*, in weight proportions (CdSe with 5%, 10%, 30%, 50%, 70%, 90%, 100%), correspondingly. The real compositions of the obtained crystals (in reference to the x values) are determined by energy dispersive X-ray spectroscopy analysis. The composition gradient along the cylinders' growth axis is negligible (less than 0.5 at. % Cd) for the considered length of samples.

The structure of most mixed crystals is determined by performing X-ray diffraction measurements at (nearly) ambient pressure onto crystal pieces ground into fine powders at the Psiché beamline of the synchrotron SOLEIL using the 0.3738 Å radiation. The X-ray diffraction lines exhibit a small linewidth (several arcseconds) throughout the composition domain, as apparent in Fig. 2. This indicates a high and stable crystal quality. The mixed crystals with moderate (3.2, 7.5, and 17.0 at. %) and large (66.5 and 88.5 at. %) Cd contents exhibit the pure-zincblende and pure-wurtzite structures, respectively. As for $Cd_{0.370}Zn_{0.630}Se$, it is dominant of the zincblende type but with a significant amount of the wurtzite structure. In fact, we have checked (not shown) that the latter crystal is anisotropic by using cross-polarized optical microscopy.

A crucial ingredient in the calculation of the Raman cross section (RCS) of the PP modes is the dispersion $n(\lambda)$ of the refractive index in the visible spectrum where the Raman scattering operates. Such dispersions measured with semi-infinite $Cd_{0.075}Zn_{0.925}Se$-c and $Cd_{0.170}Zn_{0.830}Se$-c crystals (open symbols) using a direct (model-free) wavelength-per-wavelength numerical inversion of spectrometric ellipsometry data (the sine and cosine of the depolarization angles) are shown (open symbols) in Fig. 3. An analytical form needed for $Cd_{0.075}Zn_{0.925}Se$-c was fitted to the Sellmeier formula $n^2(\lambda) = A + B \times \lambda^2 \times (\lambda^2 - \lambda_0^2)^{-1}$, with (A, B, λ_0) values of (3.916 90, 1.936 50, 351.823 30 nm) to an accuracy of $5 \times 10^{-}5$. Corresponding data for the pure-ZnSe single crystal (solid symbols), obtained by Adachi and Taguchi using the same technique,[1] and with a corresponding series of $Cd_xZn_{1-x}Se$-c/GaAs thick (∼1 μm, fully-relaxed) films analyzed by Peiris *et al.*[44] using a prism coupler technique (dashed-dotted lines), are added for comparison. In reporting the data for the films,[3] we limit ourselves to the transparency domain, i.e., to energies below the optical bandgap, of interest when performing near-forward Raman scattering measurements.

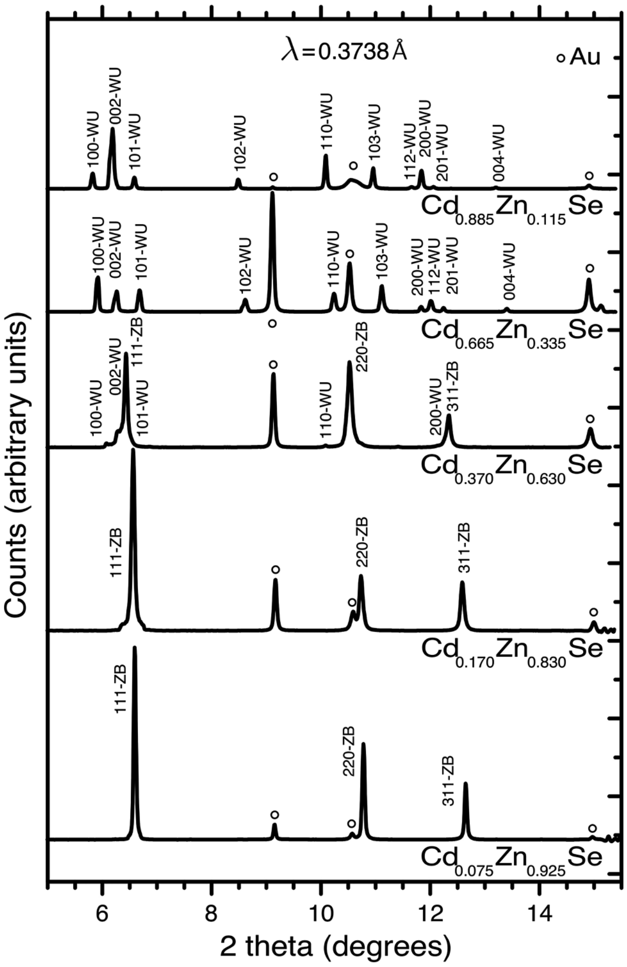

FIG. 2. X-ray $Cd_xZn_{1-x}Se$ powder diffractograms. Powder X-ray diffraction patterns obtained at (nearly) ambient pressure using the 0.3738 Å radiation (ZB, zincblende; WU, wurtzite). Circles mark diffraction lines due to Au, used for pressure calibration.

The optical bandgaps estimated at room temperature for a pure-ZnSe single crystal[1] and for a pure-ZnSe film[3] are the same (2.69 eV). The $n(\lambda)$ dispersions of the mixed crystals grown as films or single crystals are likewise consistent on the main trends: n increases with the Cd content, while its dispersion reduces with the energy. A slight overall shift of the measured curves for the single

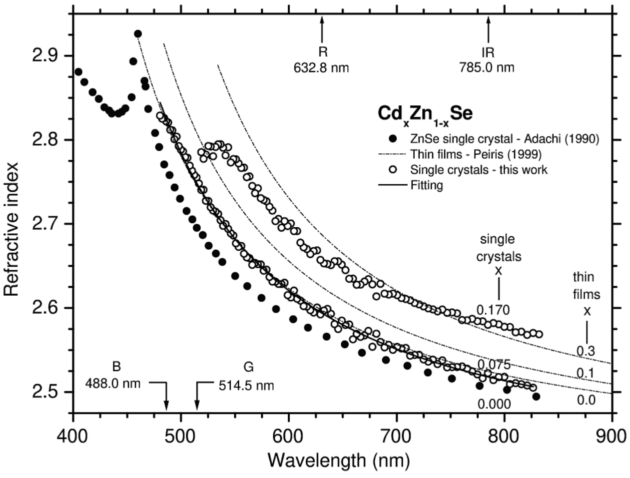

FIG. 3. Cd$_x$Zn$_{1-x}$Se-c refractive index dispersions. Refractive indices of the Cd$_{0.075}$Zn$_{0.925}$Se-c (fitted to a Sellmeier dependence—solid line) and Cd$_{0.170}$Zn$_{0.830}$Se-c single crystals (open symbols) measured by spectrometric ellipsometry. The corresponding dispersions for a ZnSe single crystal (full symbols) and from Cd$_x$Zn$_{1-x}$Se-c thin films (dashed-dotted lines) taken from Refs. 1 and 44, respectively, are added for comparison. Various laser lines are positioned.

crystals beneath those due to the films is attributed to basic differences between the two series of data. These are concerned with the sample geometry (thin films vs semi-infinite crystals) and the used optical setup (ellipsometry vs prism coupler). However, a disconcerting deviation is that the $n(\lambda)$ dispersion of the Cd$_{0.170}$Zn$_{0.830}$Se-c single crystal does not progressively converge onto the reference ZnSe one while shifting away from the optical bandgap, in contrast with all alternative $n(\lambda)$ dispersions (across films and single crystals). Such deviation reveals distinct optical properties between films and single crystals, in echo to the different phonon properties already revealed by Kozyrev (see Sec. I).[29]

The optical and vibrational deviations between films and single crystals point toward differences in the microstructures, which ultimately relate to the nature of the (Zn,Cd)-distribution as to whether this is ideally random or not.[45] Long-range ordering effects leading to a periodical modulation of the local composition in certain crystal directions are excluded in our case since additional X-ray lines reflecting such modulation besides the primitive ones due to the raw crystal lattice are not observed (Fig. 2). What remains is a trend toward short-range ordering then, in reference to local clustering or anticlustering. The X-ray diffractograms are not helpful with this respect either, since the substituent sublattice is represented by one unique site in the primitive cell of a zincblende-type mixed crystal. This produces a natural averaging over Cd- and Zn-occupancy in the X-ray data.

B. Backward/near-forward Raman measurements

Clear powder Raman spectra of the Cd$_x$Zn$_{1-x}$Se samples with zincblende/wurtzite-mixed and pure-wurtzite structures (Fig. S1 in the supplementary material)—useful to provide an overview of the phonon pattern (all the Raman-active modes show up due to the presence of all the orientations)—could be obtained only by using a near-resonant (532.0 nm) laser excitation. This leads to a spectacular enhancement of the polar LO modes and related harmonics (mediated by the Fröhlich mechanism[46]) as compared to the nonpolar TO ones, of central interest in this study (Sec. I). In fact, with the wurtzitelike powders, the TO modes are hardly distinguished at compositions away from the Zn-dilute limit. The discussion of the wurtzitelike TO modes is further complicated by the $A_1 - E_1$ lift of degeneracy due to the anisotropy of the crystal structure. Last, the signal-to-noise ratio achieved with the wurtzitelike powders is much smaller than that obtained with the pure-zincblende ones—even though the used laser line falls quite off resonance conditions in the latter case—by roughly one order of magnitude. Accordingly, our approach to achieve a refined insight into the TO mode behavior of Cd$_x$Zn$_{1-x}$Se is to focus onto the pure-zincblende crystals, namely, Cd$_{0.075}$Zn$_{0.925}$Se-c and Cd$_{0.170}$Zn$_{0.830}$Se-c, with compositions set wide apart in the zincblende domain. Single crystals are preferred to powders because they offer a possibility to address selectively the desired TO symmetry.

Polarized pure-TO Raman spectra are taken in the near-forward and backward scattering geometries through/onto (110)-oriented crystal faces obtained by cleavage in search of the PP modes and of their native TO modes, respectively. The TO and PP Raman selection rules are studied at the same sample spot, following the procedure described in Ref. 47. The polarized backward/forward Raman spectra are labeled by using Porto's notation $\vec{k}_i(\vec{e}_i, \vec{e}_s)\vec{k}_s$.[48] In this notation, the wavevectors (outside the brackets) and polarizations of the incident and scattered light, specified via explicit subscripts, are expressed in the laboratory coordinate system coinciding with the $\vec{X} = [\bar{1}10]$, $\vec{Y} = [001]$, and $\vec{Z} = [110]$ crystal axis. The experimental TO/PP Raman intensities obtained in crossed ($\perp$) and parallel ($\parallel$) polarizations depending on the azimuth angle $\alpha = (\vec{e}_i, \vec{X})$ at the sample surface are compared to the corresponding theoretical $(\vec{X}, \vec{Y})$-centered Greek crosslike and butterflylike patterns, respectively.[47] In the reported data, care was taken that the Raman signals at the start ($\alpha = 0°$) and at the end of a complete revolution ($\alpha = 360°$) are (nearly) the same, meaning that the laser is stable throughout the experiment. When needed, the scattering angle $\theta = (\vec{k}_i, \vec{k}_s)$ inside the crystal can be varied for a given $(\vec{e}_i, \vec{e}_s)$ polarization setup in the near-forward scattering geometry by slightly departing from the normal incidence ($\theta = 0°$) of the laser beam at the rear crystal face. The detection of the scattered light at the top crystal face is maintained along the fixed $\vec{Z}$ direction.

A refined contour modeling of the TO, PP, and LO Cd$_x$Zn$_{1-x}$Se Raman lineshapes is achieved by using the generic expression of the RCS given in Ref. 47. Crude approximations for the TO (and LO) modes used by Kozyrev[13,18,29] (see Sec. I) are sufficient for occasional use. However, the full expression is required for the PP modes. Otherwise, one misses important information, notably in what regards the Raman intensities (detail is given below). In any case, i.e., whether using the extended or simplified RCSs, the relative dielectric function $\varepsilon_r(\omega, x)$ of Cd$_x$Zn$_{1-x}$Se plays a central role. We adopt a classical form including an electronic background, i.e., $\varepsilon_\infty(x)$, besides Lorentzian-like contributions for the various phonon modes, p in total with p depending on the used model of phonon-mode behavior (1-mode, 2-mode, multimode, …).

Each Lorentzian is characterized by several parameters: its resonance at the p-related TO frequency, noted $\omega_{TO,p}(x)$; its damping $\gamma_p(x)$ (sample-dependent), which governs the full width at half maximum of all p-related Raman lines; and its oscillator strength $S_p(x)$, which fixes the magnitude of the p-related TO–LO splitting and also the Raman intensities of all p-type optic modes. The p-related Faust-Henry coefficient $C_{FH,p}(x)$ (ratio of the lattice to the electronic contributions to the polar vibrational modes), which comes as a weighting factor of the main $\varepsilon_r(\omega, x)$-related term in the RCS,[47] also contributes to the p-related Raman intensities.

By construction, $S_p(x)$ as well as $C_{FH,p}(x)$ scales linearly with the fraction $f_p(x)$ of the p-oscillator in the crystal. Therefore, once $f_p(x)$ is made explicit for each p-type mode within some relevant model, the $S_p(x)$ and $C_{FH,p}(x)$ dependencies come as by-products being governed by the $(\varepsilon_{\infty,}\omega_{TO}, \omega_{LO})$—(see Ref. 20) and C_{FH}—(see Ref. 49) values of the parent compounds (taken in the zincblende structure in this case), respectively. The values for ZnSe are $\varepsilon_\infty = 5.7$,[1] $\omega_{TO} = 207\ \mathrm{cm}^{-1}$,[28] $\omega_{LO} = 252\ \mathrm{cm}^{-1}$,[28] and $C_{FH} = -0.70$.[50] For the $(\omega_{TO}, \omega_{LO})$ frequencies of the CdSe-c crystal, we refer to recent *ab initio* calculations done by applying the ABINIT code to zincblende-type and wurtzite-type CdSe supercells.[51] These have demonstrated quasi-identical TO and LO Γ-like frequencies in both structures, further matching (within a few cm^{-1}) the IR values measured with the wurtzite-type CdSe crystal,[28] i.e. ($175\ \mathrm{cm}^{-1}$, $211\ \mathrm{cm}^{-1}$). The latter are thus adopted as such for CdSe-c. Besides, based on ellipsometry measurements done on a series of fully-relaxed $\mathrm{Cd}_x\mathrm{Zn}_{1-x}$Se-c epilayers, Suzuki and Adachi found that the high-frequency electronic contribution in the long-wavelength (phononlike) limit varies linearly as $\varepsilon_\infty(x) = 5.69 + 0.94x$ for $0 \leq x \leq 0.47$.[3] This gives the background electronic contribution to $\varepsilon_r(\omega, x)$ for both $\mathrm{Cd}_{0.075}\mathrm{Zn}_{0.925}$Se-c and $\mathrm{Cd}_{0.170}\mathrm{Zn}_{0.830}$Se-c and further provides a rough estimate of the ε_∞ value of CdSe-c, namely, 6.63. The only missing input parameter is the C_{FH} value for CdSe, considered as a free parameter in this work, eventually adjusted to −0.99 (see below).

Additional alloy-related input parameters are the $\omega_{TO,p}(x)$ frequencies of the three [1 × (Cd-Se), 2 × (Zn-Se)] TO modes of $\mathrm{Cd}_{0.075}\mathrm{Zn}_{0.925}$Se-c and $\mathrm{Cd}_{0.170}\mathrm{Zn}_{0.830}$Se-c identified at (193.5, 204.0, 221.5) and (191.5, 202.0, 220.0) cm^{-1}, respectively, from the Raman spectra taken in the backscattering geometry (see below).

C. *Ab initio* calculations: Siesta and AIMPRO codes

Reference *ab initio* insights into the limit $\omega_{TO,p}(x)$ frequencies of the three-TO [1 × (Cd-Se), 2 × (Zn-Se)] branches ($p = 3$) in the "ω vs x" plot of $\mathrm{Cd}_x\mathrm{Zn}_{1-x}$Se-c are gained by applying the Siesta code to prototype percolation-type impurity motifs ($x \sim 0.1$) immersed in large $2 \times 2 \times 2$- and $2 \times 2 \times 6$-replicated (hence 64- and 192-atom, respectively) zincblende-type (Cd,Zn)Se supercells. The Siesta calculations are concerned with the Γ-PhDOS that assimilates with the TO Raman signal in a crude approximation. They are done within the frozen-phonon technique after unconstrained relaxation of the supercell size and interatomic distances. The used impurity motifs are compact, i.e., at most a duo of (Zn or Cd)-cation impurities forming a short "impurity-Se-impurity" chain. They are thus well separated under the supercell-imposed periodicity, fairly representing the "isolated defect" situation.

The calculation setup, in what regards the use of the Siesta code, was described earlier, e.g., for the $\mathrm{ZnSe}_x\mathrm{S}_{1-x}$ system.[38] The norm-conserving pseudopotentials have been constructed using the scheme of Troullier and Martins[52] for the following set of nominal charge configurations and the pseudoization radii (the numbers in brackets, in Bohr units, following the corresponding electron shell label): $5s^2(2.47)5p^0(2.60)4d10(2.40)4f^0(2.40)$ for Cd, $4s^2(2.43)4p^0(2.37)3d10(2.10)4f^0(2.82)$ for Zn, and $4s^2(1.90)4p^4(2.00)3d10(1.20)4f^0(1.50)$ for Se. The basis functions of the "double-zeta with polarization orbitals" quality were generated using the "energy shift" parameter, which controls in Siesta the confinement of the basis functions, equal to 5 mRy. This resulted in the following values of the maximal extension of strictly confined orbitals (the most protruded ones on each atom): 3.72 Å for Zn, 3.83 Å for Cd, and 3.36 Å for Se. The exchange-correlation was treated within the local density approximation (LDA), whereby no special effort was taken to correct for the bandgap value. The force constants in phonon calculations were slightly overestimated, resulting in a slight upward drift of the calculated frequencies by $\sim 15\ \mathrm{cm}^{-1}$, as compared to experimental results. The k-sampling was done over $2 \times 2 \times 2$ divisions of the (cubic) Brillouin zone of the supercell, which was tested to yield sufficient accuracy in the calculation of forces.

An *ab initio* insight into the relative Raman intensities of the two ZnSe-like TO modes was further needed to elucidate the sensitivity (up to first- or second-neighbors) of the Zn-Se vibration to its local ZnSe- (lower mode in the percolation scheme) or CdSe-like (upper mode) environment. This was gained via a direct *ab initio* calculation of the $\mathrm{Cd}_x\mathrm{Zn}_{1-x}$Se Raman spectrum at intermediary compositions ($x = 0.5$ and 0.3), where both types of environments are well represented. For doing so, we applied the AIMPRO code onto large 216-atom zincblende supercells—which appeared to be sufficiently converged in size for such purpose. The AIMPRO density functional theory calculations were done within the LDA for the exchange-correlation potential by Perdew and Wang,[53] taking the norm-conserving pseudopotentials for Cd, Zn, and Se as proposed by Hartwigsen *et al.*[54] The 3*d* and 4*d* electrons were taken into account explicitly as valence electrons for Zn and Cd, respectively. Kohn-Sham orbitals were expanded in atom-centered *s*, *p*, and *d* cartesian-gaussian functions. The Brillouin zone of the 216-atom cubic supercells was sampled by a $2 \times 2 \times 2$ special k-point mesh as proposed by Monkhorst and Pack[55] using a third-order Birch-Murnaghan[56] equation of state. This approach gives $a = 0.559$ (0.602) nm, $B_0 = 68.6$ (60.3) GPa, and $B' = 4.4$ (4.5) for ZnSe (CdSe-c), respectively. These theoretical values are in reasonable agreement with the ZnSe (CdSe-c) experimental data of $a = 0.567$ (0.605) nm, $B_0 = 63$ (53) GPa, and $B' = 4.77$, respectively.[57–60]

The *ab initio* Raman cross section was calculated following de Gironcoli,[61]

$$\sigma^{xy}(\omega) \propto \sum_{\nu} \frac{\delta(\omega_\nu - \omega)}{\omega_\nu} \left| \sum_i s_i\, u^{\nu}_{iz} \right|^2,$$

where ν runs over all phonon modes, ω_ν is the frequency of the ν mode, u^{ν}_{iz} is the z component of the displacement of the atom at the lattice site i and mode ν, and s_i is +1 and −1, depending on whether the site i belongs to the cationic or anionic *fcc* sublattice, respectively. $\delta(\omega_v - \omega)$ was considered to be a $2\,\mathrm{cm}^{-1}$-broad Lorentzian function. The AIMPRO code calculates the second-order partial derivatives of the total energy with respect to the atomic coordinates at equilibrium positions. The frequencies and the normal modes were obtained by diagonalization of the dynamical matrix. The equilibrium configurations were determined after an exhaustive full relaxation (atom positions and lattice parameter), until the maximum force was $2\ \mathrm{meV/\mathring{A}}$. The AIMPRO code uses downhill simplex optimization to minimize the total energy with respect to the lattice parameter and a conjugate gradient method to relax the atomic positions.[41] For the parent crystals ZnSe and CdSe-c, the calculated TO Raman frequencies of $219.8\,\mathrm{cm}^{-1}$ and $180.0\,\mathrm{cm}^{-1}$, respectively, are in good agreement with the available experimental data for ZnSe[62] ($205\,\mathrm{cm}^{-1}$) and other *ab initio* calculations for c-CdSe ($198\,\mathrm{cm}^{-1}$—Ref. 63 and $172\,\mathrm{cm}^{-1}$—Ref. 51).

An ordering parameter κ $(-1 \leq \kappa \leq +1))$ was introduced to monitor the nature of the Zn ↔ Cd substitution in a given (Cd,Zn)Se supercell, as to whether this is ideally random ($\kappa = 0$) or due to clustering ($\kappa > 0$) or anticlustering ($\kappa < 0$). The desired κ value was adjusted using a simulated annealing algorithm detailed in Ref. 64, in the same spirit as early done for the diamond-type $\mathrm{Ge}_x\mathrm{Si}_{1-x}$ mixed crystal.[65] At each annealing step of a given (Cd,Zn)Se supercell, the five possible Se-centered tetrahedral units (with Zn and/or Cd at the vertices) were counted. The κ value was deduced from a comparison with the predicted κ-dependent fractions derived from the binomial Bernoulli distribution[66] (the bond counting procedure used in Ref. 65 was not relevant for the present case since the bond fraction is not κ-dependent in a zincblende-type mixed crystal). Note that with the used 216-atom supercells, a reliable crystal structure could not be obtained for κ values greater than 0.4.

Certainly, our method to adjust the κ value of a given supercell is not as sophisticated as that developed by Zunger *et al.*[67] to design their special quasirandom structures (SQSs), which reproduces correlations up to a very large length scale. Still, the pair and multiple correlation functions of our large 216-atom random ($\kappa \sim 0$) $\mathrm{Cd}_{54}\mathrm{Zn}_{54}\mathrm{Se}_{108}$ supercell calculated up to fourth-neighbors along the method of Wei *et al.*,[68] displayed as Table S1 in the supplementary material, are quite correct. This, anyway, is sufficient for our use since, apparently, the sensitivity of the bond vibrations to their local environment does not exceed the second-neighbors in $\mathrm{Cd}_x\mathrm{Zn}_{1-x}\mathrm{Se}$-c (see below). Also, the current method conveniently applies to design random ($\kappa \sim 0$) as well as nonrandom ($\kappa \neq 0$) zincblende-type supercells, as needed for the current study.

III. PERCOLATION-TYPE PHONON-MODE BEHAVIOR OF $\mathrm{Cd}_x\mathrm{Zn}_{1-x}$Se-C: THE *AB INITIO* INSIGHT

In preamble to the *ab initio* calculations, we report in Fig. 1 an overview of representative $\mathrm{Cd}_x\mathrm{Zn}_{1-x}\mathrm{Se}$ TO (full symbols) and LO (open symbols) IR and Raman data taken from Refs. 28 (squares, read from Fig. 4 therein) and 24 (crosses, read from Fig. 7 therein) using single crystals and thin films, respectively. Our current Raman data obtained with the ZnSe, $\mathrm{Cd}_{0.032}\mathrm{Zn}_{0.968}$Se-c, $\mathrm{Cd}_{0.075}\mathrm{Zn}_{0.925}$Se-c, and $\mathrm{Cd}_{0.170}\mathrm{Zn}_{0.830}$Se-c single crystals (triangles) are superimposed. The frequency of the CdSe:Zn impurity mode (x~0) predicted by Kozyrev[18] using Green's function completes the picture (marked by a star). Altogether, an overall three-mode TO pattern (thick/straight lines) is revealed.

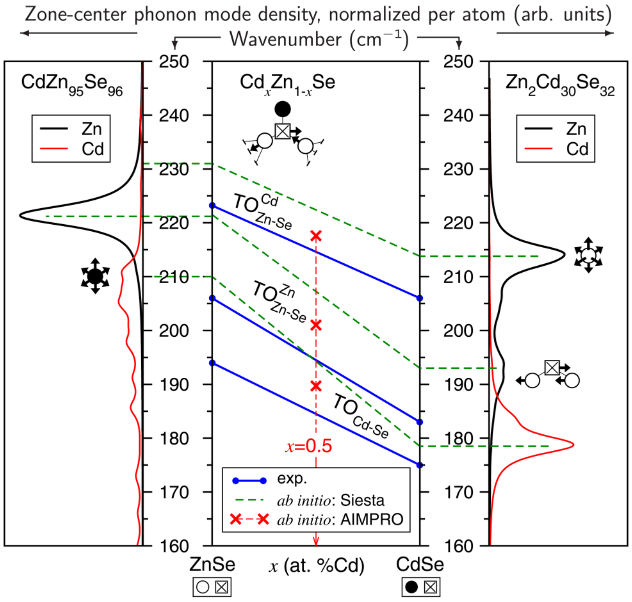

FIG. 4. *Ab initio* insight into the end (($x \sim 0.1$) TO frequencies of the $\mathrm{Cd}_x\mathrm{Zn}_{1-x}$Se-c percolation scheme. Limit frequencies of the three [1 × (Cd-Se), 2 × (Zn-Se)] $\mathrm{Cd}_x\mathrm{Zn}_{1-x}$Se-c TO branches obtained by applying the Siesta code to prototype impurity motifs in large supercells (64- and 192-atom). The related Γ-PhDOS per Zn (black curves) and Cd (red curves) atoms flank the main panel. The limit frequencies are extrapolated into linear variations (dashed lines). The experimental branches (taken from Fig. 1) are added for comparison (full lines). The crosses at $x = 0.5$ represent TO frequencies used in Fig. 5.

The TO modes are labeled using the percolation terminology $\{TO_{\mathrm{Cd\text{-}Se}}, TO^{\mathrm{Zn}}_{\mathrm{Zn\text{-}Se}}, TO^{\mathrm{Cd}}_{\mathrm{Zn\text{-}Se}}\}$ in which the subscript and the superscript refer to a bond vibration and to its local environment, respectively. The polar LO modes couple via their long-range electric field and thus can be assigned neither to a specific bond nor to a specific environment. They are merely labeled as $\{LO^{-}, LO^{int}, LO^{+}\}$ in order of increasing frequency. We discuss briefly in Sec. II of the supplementary material how the three-mode TO pattern apparent in Fig. 1 can be anticipated based on the contrasts in bond physical properties (length, reduced masses, size of substituent) of $\mathrm{Cd}_x\mathrm{Zn}_{1-x}$Se.

A. *Ab initio* insight into the (TO) frequencies ($x \sim 0.1$)—Siesta code

In this section, the three-TO $\mathrm{Cd}_x\mathrm{Zn}_{1-x}\mathrm{Se}$ percolation pattern of Fig. 1 is put to the *ab initio* test. The percolation model is a phenomenological one based on a description of the lattice at one dimension (1D) along the linear chain approximation. Accordingly, we transpose to 1D the discussion of the actual three-dimensional (3D) vibration patterns revealed by the *ab initio* calculations.

Relevant supercells to explore the end frequencies of the Zn-Se (×2) and Cd-Se (×1) branches are a 64-atom $(2 \times 2 \times 2)$ CdSe-like one containing a Zn-duo $(x \sim 0)$ and an elongated 192-atom $(2 \times 2 \times 6)$ ZnSe-like one containing an isolated Cd-impurity $(x \sim 1)$, respectively. The related Γ-PhDOS per Zn (black curves) and Cd (red curves) atoms obtained with the Siesta code are shown on the left and right hand sides of the main panel in Fig. 4, respectively.

The CdSe and ZnSe parent modes (large symbols) due to vibrations of the host lattices away from the impurity motifs show up at ∼178 cm^{-1} and ∼221 cm^{-1}, respectively.

The Zn-duo in CdSe provides the end frequencies of both Zn-Se branches at $x \sim 1$. The stretching along the short Zn-Se-Zn chain naturally refers at 1D to the Zn-Se vibration in the ZnSe-like environment. The related CdSe:2Zn impurity mode shows up at ∼193 cm^{-1}. All variants in bending of the Zn-Se-Zn chain (five in total) are discussed at 1D in terms of Zn-Se stretching outside the chain, i.e., in the CdSe-like environment. We have checked (not shown) that the chain-bending modes are degenerated (within ∼2 cm^{-1}) with the CdSe:Zn impurity mode due to an isolated Zn-impurity in CdSe, emerging at ∼214 cm^{-1}.

An insight into the Zn-Se doublet at $x \sim 0$ is more challenging since Zn-Se is the host species in this case. The localization of any ZnSe-like impurity mode is thus difficult to appreciate. The problem is solved by designing an elongated $2 \times 2 \times 6$ (192-atom) supercell with a single Cd impurity, which offers enough space, at least in one dimension, to discriminate the vibration patterns over the Zn-Se bonds immediately close to Cd (upper Zn-Se mode) or more distant from it (lower Zn-Se mode). The related ZnSe/Cd impurity mode (localized Zn-Se vibration around Cd) and parent ZnSe mode are accordingly identified at ∼231 cm^{-1} and ∼220 cm^{-1}, respectively. In fact, the ZnSe/Cd impurity mode refers to the collective in-phase (quasispherical) displacement of the Zn atoms (12 in total) forming the first-neighbor shell of the Cd-impurity against the Se atoms (4 in total) to which they are bonded (a fragmental view is sketched out in the main panel of Fig. 4).

The Cd-like Γ-PhDOS reveals an isolated vibration of Cd against Se in the ZnSe-like medium at ∼210 cm^{-1}, assigned as the ZnSe:Cd impurity mode (isolated Cd-Se vibration in ZnSe). The latter conveniently falls inside the rather narrow gap (∼35 cm^{-1}) separating the acoustic and optic bands of the host ZnSe PhDOS.[69] As such, it consists of an actual gap mode, likely to show up as a distinct feature in the Raman/IR spectra. Kozyrev arrived at the same conclusion via the Green's function calculation.[18]

If we omit a slight LDA-induced upward drift of all phonon frequencies (Sec. II C), the current *ab initio* insight into the end frequencies (connected via dashed lines in Fig. 4) of the three [1 × (Cd-Se), 2 × (Zn-Se)] TO branches of Fig. 1 (thick lines in Fig. 4) consistently supports their percolation-type assignment in terms of $\{TO_{\text{Cd-Se}}, TO^{\text{Zn}}_{\text{Zn-Se}}, TO^{\text{Cd}}_{\text{Zn-Se}}\}$.

B. *Ab initio* (TO) Raman spectrum of the random crystal ($x \sim 0.5$)—AIMPRO code

The lacking *ab initio* insight into the TO Raman intensities is gained by applying the AIMPRO code to a large (216-atom) zinc-blende $Zn_{54}Cd_{54}Se_{108}$ $(x = 0.5)$ supercell corresponding to a random Zn ↔ Cd substitution optimized by simulated annealing (Sec. II C). The resulting *ab initio* TO Raman spectrum is shown in Fig. 5 (dashed curve). The "pseudo" Raman signal (symbols) reconstructed by Kozyrev at a close composition by taking the imaginary part of $\varepsilon_r(\omega, x)$ (see Sec. I) is added for comparison (symbols, digitized from Fig. 1 of Ref. 18). In this case, $\varepsilon_r(\omega, x)$ was derived from a model-independent Kramers-Krönig transformation of the raw $Cd_{0.45}Zn_{0.55}Se$ IR-reflectivity spectrum. As ideally expected, three main contributions in the "experimental-like" data of Kozyrev (at ∼180, ∼195, and ∼208 cm^{-1}), presumably referring to the percolation-type $(TO_{\text{Cd-Se}}, TO^{\text{Zn}}_{\text{Zn-Se}}$, and $TO^{\text{Cd}}_{\text{Zn-Se}})$ features, are echoed by *ab initio* replicas (at ∼190, ∼203, and ∼216 cm^{-1}). The LDA-shift is artificially compensated in Fig. 5 for a better comparison.

A careful contour modeling of the *ab initio* three-mode Raman signal using Gaussian functions reveals that the $TO^{\text{Zn}}_{\text{Zn-Se}}$ mode is roughly three times larger than $TO^{\text{Cd}}_{\text{Zn-Se}}$. Such ∼3:1 intensity ratio reveals a sensitivity of the Zn-Se vibration to its local environment at the next-neighbor scale.[38] This makes a distinction between, on the one hand, the pure-Zn environment taken together with

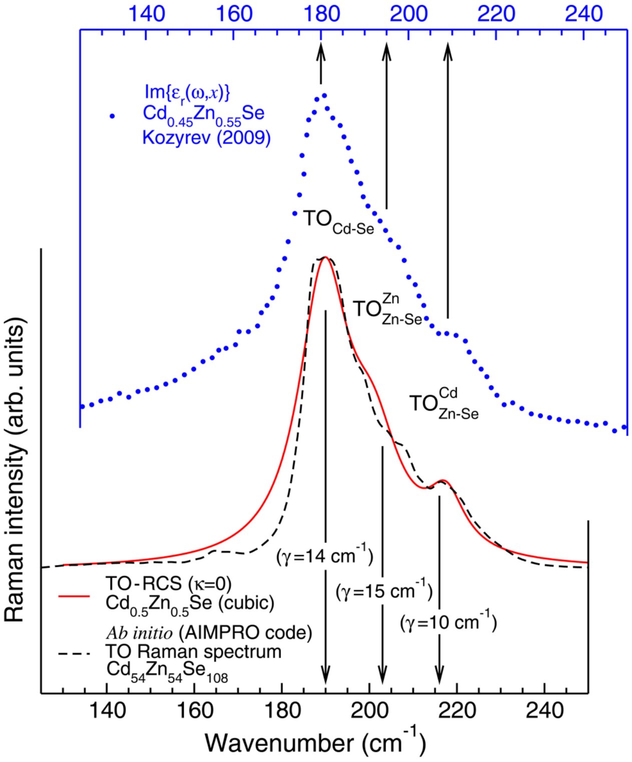

FIG. 5. *Ab initio* insight into the TO Raman intensities of random $Cd_{0.5}Zn_{0.5}Se$-c. *Ab initio* TO Raman spectrum obtained by applying the AIMPRO code to a random $(\kappa = 0)$ $Cd_{54}Zn_{54}Se_{108}$ cubic supercell (dashed line). The corresponding TO-RCS (solid line) obtained by using the TO-frequencies and *f*-terms given in Fig. 1 is superimposed for comparison. The used γ_p dampings are specified. The $\mathrm{Im}\{\varepsilon_r(\omega, x = 0.45)\}$ spectrum (shifted horizontally) reconstructed from IR-reflectivity data (Ref. 18) is shown (symbols) for reference purpose.

the (Cd,Zn)-mixed ones and, on the other hand, the pure-Cd environment, respectively. The corresponding 1D-oscillators express as {ZnSe(Zn-Se)ZnSe, 2 × CdSe(Zn-Se)ZnSe} and CdSe (Zn-Se)CdSe, with respective fractions $f^{\text{Zn,(Zn,Cd)}}_{\text{Zn-Se}}(x) = f^{\text{Zn}}_{\text{Zn-Se}}(x) = (1-x)^3 + 2x(1-x)^2$ and $f^{\text{Cd}}_{\text{Zn-Se}}(x) = (1-x)x^2$, assuming a random Zn ↔ Cd substitution. With this, intensity matching between the two Zn-Se TO submodes occurs at $x \sim 0.7$. As for the $TO_{\text{Cd-Se}}$ mode, which remains blind to its local environment, the relevant 1D-oscillator is "(Cd-Se)," whose fraction in the crystal is $f_{\text{Cd-Se}}(x) = x$. The f-terms are incorporated in Fig. 1 to complete the $\text{Cd}_x\text{Zn}_{1-x}$Se-c version of the percolation scheme. In fact, the three-mode $\{TO_{\text{Cd-Se}}, TO^{\text{Zn}}_{\text{Zn-Se}}, TO^{\text{Cd}}_{\text{Zn-Se}}\}$ TO-RCS (solid curve in Fig. 5) calculated for $\text{Cd}_{0.5}\text{Zn}_{0.5}$Se with the $\omega_{TO,p}(x)$ (upward shifted by $5.0 \pm 1.5\,\text{cm}^{-1}$ to compensate the LDA-overestimate—see Sec. II C) and $f_p(x)$-terms ($p = 3$) given in Fig. 1 mimic fairly well the *ab initio* Raman spectrum. Only the $\gamma_p(x)$ dampings were adjusted, to the specified values therein.

C. IR-based vs *ab initio*-based TO and LO Raman lineshapes

An overview of the three-mode [1 × (Cd-Se), 2 × (Zn-Se)] TO-RCS and LO-RCS obtained for random $\text{Cd}_x\text{Zn}_{1-x}$Se-c by using the $\omega_{TO,p}(x)$ values (thick lines) and $f_p(x)$-terms given in Fig. 1 is shown in Fig. 6. A minimal damping γ_p ($1\,\text{cm}^{-1}$) is taken, for optimal resolution of neighboring features. The curves corresponding to the available crystal compositions ($x = 0.075$ and 0.170) and to the zincblende ↔ wurtzite structural transition ($x = 0.3$) are highlighted. The resulting LO frequencies are reported in Fig. 1 (thin lines).

We further report in Fig. 1 the LO frequencies calculated by considering a sensitivity of the Zn-Se vibration reduced to the first-neighbors (dashed lines), just as an aside. In this case, the relevant 1D-oscillators behind the $TO^{\text{Zn}}_{\text{Zn-Se}}$ and $TO^{\text{Cd}}_{\text{Zn-Se}}$ submodes take the compact Se(Zn-Se)Zn and Se(Zn-Se)Cd forms. The corresponding fractions in the crystal are x^2 and $2x(1-x)$, assuming a random Zn ↔ Cd substitution. In this (virtual) case, the intensity matching between the two Zn-Se TO modes is expected at $x \sim 0.5$ and not at $x \sim 0.7$ (sensitivity at the second-neighbor scale). Note that both the LO^+ frequency and the inverted LO–TO splitting of the upper/minor in-band mode dramatically enlarge when shifting from the second-neighbor description to the first-neighbor one. This is especially true in the zincblende domain of current interest.

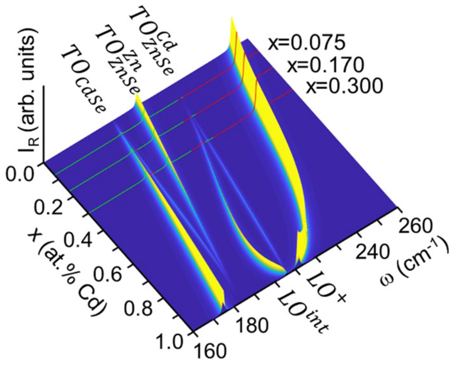

FIG. 6. Theoretical (TO,LO) Raman lineshapes for random $\text{Cd}_x\text{Zn}_{1-x}$Se-c. Theoretical TO-RCS and LO-RCS derived for the random $\text{Cd}_x\text{Zn}_{1-x}$Se-c system by using the TO-frequencies and f-terms given in Fig. 1. The x values studied in this work and corresponding to the zincblende → wurtzite structural transition ($x \sim 0.3$) are emphasized. Small $\gamma_p(x)$ values ($1\,\text{cm}^{-1}$) are taken for clarity.

Whether considering the (virtual) first-neighbor or (actual) second-neighbor description, the theoretical LO^{int} frequencies underestimate the experimental values to a point that a finite $LO^{int} - TO^{\text{Cd}}_{\text{Zn-Se}}$ inversion (beyond the experimental detection limit) is predicted for the minor in-band mode from 10 at. % Cd and above. This contradicts the quasidegeneracy apparent in the IR data throughout the zincblende domain (even up to 40 at. % Cd).[28] The reason for such abnormally small $LO^{int} - TO^{\text{Cd}}_{\text{Zn-Se}}$ inversion apparent in the available IR data in the literature is discussed hereafter in the light of a pure-TO Raman study of $\text{Cd}_x\text{Zn}_{1-x}$Se-c mixed crystals.

IV. TO-LIKE RAMAN STUDY OF $\text{Cd}_x\text{Zn}_{1-x}$Se-C

In this section, we develop a pure-TO Raman study of the apparent three-mode pattern of $\text{Cd}_x\text{Zn}_{1-x}$Se-c, with special attention to its lower and upper/minor features, assigned as $TO_{\text{Cd-Se}}$ and $TO^{\text{Cd}}_{\text{Zn-Se}}$ in the percolation scheme, respectively. First, we study the Raman selection rules of the main $TO^{\text{Zn}}_{\text{Zn-Se}}$ feature to assess the overall "quality" of the $\text{Cd}_x\text{Zn}_{1-x}$Se TO Raman signal in its x-dependence.

A. Symmetry analysis of the central/dominant $TO^{\text{Zn}}_{\text{Zn-Se}}$ mode: Backward scattering

The Raman spectra taken with $\text{Cd}_{0.075}\text{Zn}_{0.925}$Se-c and $\text{Cd}_{0.170}\text{Zn}_{0.830}$Se-c ground as fine powders (top curves) by using a nonresonant (632.8 nm, see Fig. 3) laser line in the backscattering geometry are shown in Figs. 7(a) and 7(b), respectively. Due to the lack of symmetry when using powders, the TO modes come together with the LO modes and with the spurious second-order two-phonon (2A) zone-edge bands (top curves). The (allowed) TO signal is cleared from the (forbidden) LO modes when implementing the backscattering geometry onto (110)-oriented cleaved faces of single crystals. Furthermore, in this case, the spurious 2A-band can be drastically reduced (central curves) and eventually eliminated (bottom curves) by adopting the polarized $Z(XX)\bar{Z}$ and $Z(XY)\bar{Z}$ scattering geometries, respectively.

The suppression of the 2A-band clarifies the Raman signal on the low-frequency side of the main TO feature (opposite arrows in Fig. 7(a) emphasize a change in the Raman signal). This reveals a bimodal fine structure at both studied compositions. The fine structure survives the disappearance of the 2A-band. We conclude that it is intrinsic to $\text{Cd}_x\text{Zn}_{1-x}$Se-c and not (entirely) due to the Fano-like interference with the 2A-band as originally proposed by Valakh *et al.*[21–23] The main/upper component of the fine structure reinforces at the expense of the minor/lower one when the Cd content decreases. This is consistent with their percolation-type assignment in terms of $TO^{\text{Zn}}_{\text{Zn-Se}}$ and $TO_{\text{Cd-Se}}$, respectively. In fact, the two theoretical TO-RCS calculated on this basis [using the $f_p(x)$-terms given in Fig. 1] for $\text{Cd}_{0.075}\text{Zn}_{0.925}$Se-c and $\text{Cd}_{0.170}\text{Zn}_{0.830}$Se-c (thin curves in the left insets of Fig. 7) fairly

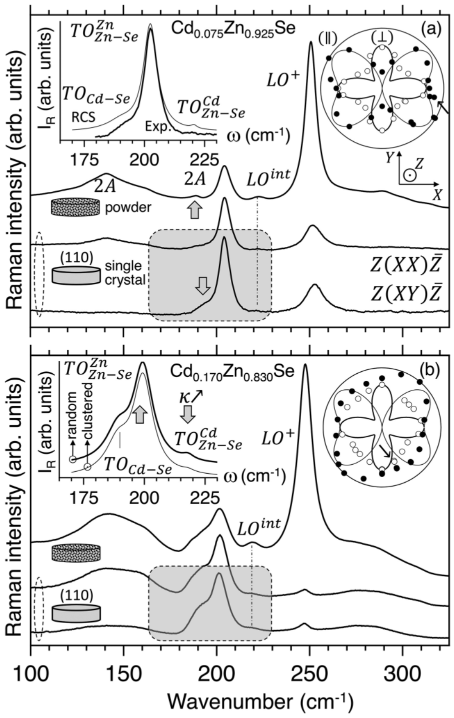

FIG. 7. Backward TO and LO Cd$_x$Zn$_{1-x}$Se-c Raman spectra. Unpolarized/polarized (TO,LO)/pure-TO Cd$_{0.075}$Zn$_{0.925}$Se-c (a) and Cd$_{0.170}$Zn$_{0.830}$Se-c (b) backscattering Raman spectra (632.8 nm laser line) using powders (upper curves) and (110)-faces of single crystals (lower curves). Right insets: symmetry analysis of the dominant $TO^{Zn}_{Zn\text{-}Se}$ mode in crossed (⊥, open symbols) and parallel (||, full symbols) polarizations. The Raman intensities (normalized to the maximum value in each series) match over a complete revolution (360°) of the (⊥,||)-polarization pairs at the sample surface (as emphasized by arrows). The theoretical Greek crosslike (⊥, thick curve) and butterflylike (||, thin curve) patterns are shown for comparison. Left insets: TO-RCS of the random ($\kappa = 0$, panels a and b) and/or clustered ($\kappa = 0.5$, panel b) systems to compare with the pure-TO experimental Raman signals in the shaded boxes. The Raman signal in the box of panel a is replicated in the left inset (lower curve) for a direct comparison with the TO-RCS (upper curve).

well reproduce the corresponding experimental Raman signals (bottom curves in both panels of Fig. 7, replicated in the inset of Fig. 7(a), for a direct comparison with the TO-RCS).

We have checked (not shown) that $TO_{\text{Cd-Se}}$ remains located at a lower frequency than $TO^{\text{Zn}}_{\text{Zn-Se}}$ at $x = 0.032$ (Fig. 1), i.e., even in the Cd-dilute limit. This supports an assignment of the ZnSe:Cd impurity mode in terms of an actual gap mode falling beneath the host ZnSe-like TO–LO band at $x \rightarrow 0$, and not inside it, as believed for a long time (Sec. I). This is moreover consistent with our current *ab initio* calculations (arrows, Fig. 1) and also with calculations based on Green's functions done by Kozyrev (star, Fig. 1).[18]

At this stage, a detailed symmetry analysis of the TO Raman signal focused on the main $TO^{\text{Zn}}_{\text{Zn-Se}}$ feature is useful to decide which crystal out of Cd$_{0.075}$Zn$_{0.925}$Se-c and Cd$_{0.170}$Zn$_{0.830}$Se-c is best suited to test further the nature of the presumed $TO_{\text{Cd-Se}}$ mode by near-forward Raman scattering (see Sec. IV B).

In the right insets of Fig. 7, the $TO^{\text{Zn}}_{\text{Zn-Se}}$ modes of both mixed crystals globally adhere to the theoretical Greek crosslike (thick curves) and butterflylike (thin curves) patterns in crossed (open symbols, ⊥) and parallel (solid symbols, ||) polarizations. Such patterns are fairly well reproduced with Cd$_{0.075}$Zn$_{0.925}$Se-c but not with Cd$_{0.170}$Zn$_{0.830}$Se-c. The significant deviation at $x = 0.170$ is not due to the increased alloy disorder as compared to $x = 0.075$, since the TO modes of the alternative ZnSe-based Zn$_{1-x}$Be$_x$Se-c mixed crystal ideally obey the nominal Raman selection rules even at $x \sim 0.50$ (corresponding to the maximum alloy disorder),[47] though the contrast in bond physical properties (bond length and covalency) is larger than with Cd$_x$Zn$_{1-x}$Se.[11,70] The deviation is rather attributed to the persisting Fano-like interference of $TO^{\text{Zn}}_{\text{Zn-Se}}$ with the 2A-band nearby, which cannot be fully suppressed.

B. Phonon-polariton insight into the lower $TO_{\text{Cd-Se}}$ mode: Near-forward scattering

In this section, we explore the PP regime of Cd$_x$Zn$_{1-x}$Se by near-forward scattering, using Cd$_{0.075}$Zn$_{0.925}$Se-c as a case study. It is a matter to achieve a decisive experimental evidence as to whether the shoulder apparent on the low-frequency tail of the main/central $TO^{\text{Zn}}_{\text{Zn-Se}}$ modes of Cd$_{0.075}$Zn$_{0.925}$Se-c and Cd$_{0.170}$Zn$_{0.830}$Se-c (Fig. 7) consists of the actual Γ-like $TO_{\text{Cd-Se}}$ mode—as we believe along with Kozyrev[29] or is merely due to a Fano-like distortion of the main TO signal as originally advanced by Valakh *et al.*[21–23] The latter option cannot be excluded in view of the imperfect Raman selection rules (Sec. IV A).

When entering the PP regime, close TO modes couple via their developing transverse (photonlike) electric field, resulting in a massive transfer of oscillator strength toward low frequency—and not toward high frequency as for LO modes.[37,38] Consequently, if the shoulder can be actually identified with $TO_{\text{Cd-Se}}$, an interbond $TO^{\text{Zn}}_{\text{Zn-Se}} \rightarrow TO_{\text{Cd-Se}}$ transfer of oscillator strength is expected, which should naturally put $TO_{\text{Cd-Se}}$ into focus (as the recipient of oscillator strength). Otherwise, if the shoulder is merely due to a Fano-distortion of the main TO mode, no significant transfer of oscillator strength should occur. This is because the latter mode, trapped by the Fano interference, would fail to enter fully its PP regime, as independently observed with the alternative ZnSe-based ZnSe$_{1-x}$S$_x$,[38] Zn$_{1-x}$Be$_x$Se,[71] and Zn$_{1-x}$Mg$_x$Se[72] systems. Only "fractional" PP modes carrying a small amount of oscillator strength are likely to radiate in this case, if any.

Optimal conditions for the planned near-forward Raman study of Cd$_{0.075}$Zn$_{0.925}$Se-c are searched for by computing its three-mode [1 × (Cd-Se), 2 × (Zn-Se)] PP-RCS in its (ω, q)-dependence. We use the generic formula given in Ref. 47. The resulting ω vs y three-PP (PP^-, PP^{int}, PP^+) dispersion[73] is shown in Fig. 8(a). $y = \frac{q \cdot c}{\omega_1}$ is a dimensionless parameter that conveniently substitutes for q (after division by ω_1 that arbitrarily refers to the TO frequency of pure ZnSe).

Im$\{\varepsilon_r(\omega, x)\}$ constitutes a reasonable approximation of the RCS for the asymptotic TO modes behind the PP ones (Sec. I),[13,18,29] but not for the PP modes themselves. This is especially true in what regards the Raman intensities that are primarily impacted by any transfer of oscillator strength—thus of crucial interest for our concern. In fact, Im$\{\varepsilon_r(\omega, x)\}$ totally misses the photonlike extinction

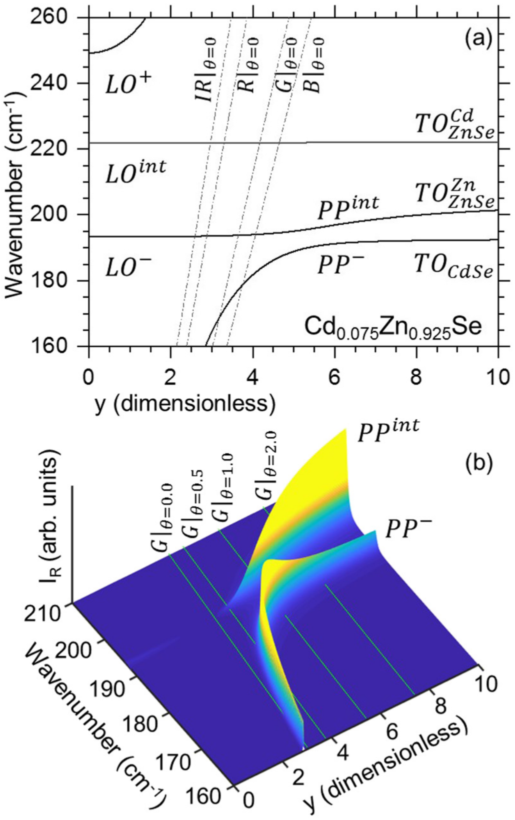

FIG. 8. $Cd_{0.075}Zn_{0.925}Se$-c PP regime. Theoretical dispersion (a) and the Raman signal (b) of the $Cd_{0.075}Zn_{0.925}Se$-c PP modes. The Raman scan lines calculated in the perfect forward scattering geometry ($\theta = 0°$) by using the dispersion of the refractive index (Fig. 3) close to the near-infrared (IR, 785.0 nm), red (R, 632.8 nm), green (G, 514.5 nm), and blue (B, 488.0 nm) laser lines (panel a) and in various near-forward scattering geometries ($\theta \sim 0°$) using the green laser line (panel b) are superimposed.

of the central PP^{int} branch, a pivotal feature at the heart of the strong PP-coupling regime, on both sides of which the PP^{int} Raman intensity dramatically changes. In the present case, the extinction occurs close to the bottleneck created by the mutual repulsion of the PP^{-} ($TO_{\text{Cd-Se}}$-related) and PP^{int} ($TO^{\text{Zn}}_{\text{Zn-Se}}$-related) branches in tight coupling. As apparent in Fig. 8(b), a dramatic $PP^{int} \rightarrow PP^{-}$ transfer of oscillator strength occurs in this bottleneck region. The originally minor PP^{-} feature away from Γ strengthens by almost one order of magnitude at the expense of the PP^{int} one, which concomitantly vanishes to zero. Note that the PP^{-} strengthening is clearly a transient feature; it develops and disappears within less than half a unit on the y-scale. Therefore, its detection by Raman scattering is a real challenge.

In Fig. 8(a), the ω vs y dispersions scanned by near-forward Raman scattering at a minimal scattering angle ($\theta = 0°$) with the well-spanned near-infrared (IR-785.0 nm), red (R-632.8 nm), green (G-514.5 nm), and blue (B-488.0 nm) laser lines throughout the visible spectrum are superimposed (dotted lines) onto the theoretical PP dispersion (solid lines). This is required to assess which laser excitation is best suited to probe the sensitive bottleneck region. We recall that the "Raman scan lines" stem from the wavevector conservation law governing the Raman scattering once developed in its θ-dependence. For doing so, we express the magnitudes of the incident (laser) and scattered (light) wavevectors using the dispersion of the refractive index of the crystal around the used laser line (Sec. II). The most energetic (B) laser line falls short of covering the bottleneck region in full. It is anyway absorbed by the crystal (thus inappropriate for any "transmissionlike" measurement) due to near-resonance conditions (Fig. 3). In contrast, the less energetic (IR and R) lines—for which the crystal is transparent—penetrate deep into the PP dispersion, i.e., much beyond the photonlike extinction of PP^{-}. Therefore, they exceed by far the sensitive bottleneck region. Moreover, such lines are hampered by a poor signal-to-noise ratio due to the ω^4-scaling of the Raman efficiency. This leaves the green (G) laser line as the best candidate to probe the bottleneck region. In fact, as shown in Fig. 8(b), the G-related Raman scan lines spanning small θ angles in the range 0–2° (clear curves) suffice to cover in full the strong $PP^{-} \leftrightarrow PP^{int}$ coupling regime, down to complete (photonlike) extinction of the PP^{-} mode. This is ideal for our concern.

A selection of nominally pure-TO near-forward Raman spectra taken at the same sample spot with the G laser line at various near-normal incidences ($\theta \sim 0°$) onto parallel (110)-oriented crystal faces of a cleaved $Cd_{0.075}Zn_{0.925}Se$-c crystal piece is displayed in Fig. 9. The 2A-band likely to Fano-interfere destructively with any $TO_{\text{Cd-Se}}$-related PP is minimized by using crossed polarizations of the incident and scattered lights at $\alpha \sim 0°$ (Sec. IV A). Though theoretically forbidden, the LO modes show up strongly, due to multireflection of the laser beam between the parallel crystal faces.[74] Moreover, the backscatteringlike TO signal generated by the laser beam after reflection on the top crystal face superimposes onto the near-forward PP one created by the laser beam on its way forth to the same face. The Raman spectrum taken at the same sample spot in the backscattering geometry (top-thick curve) is added for reference purpose.

Decreasing θ, the originally minor ($\theta \sim 180°$) shoulder apparent on the low-frequency tail of the main $TO^{\text{Zn}}_{\text{Zn-Se}}$ feature progressively softens while developing into a strong band. Eventually (at $\theta \sim 0°$), this becomes comparable in magnitude with the reference backscattering signal, as expected in the bottleneck region [Fig. 8(b)]. Moreover, the strong band ($\theta \sim 0°$) obeys the nominal Raman selection rules of a TO mode (Fig. 9, inset)—the full series of polarized Raman spectra is provided as Fig. S2 in the supplementary material. Altogether, the θ-dependence and symmetry analysis of the Raman band activated by near-forward scattering ascertain its PP character. Therefore, its native shoulder observed in the backscattering geometry can safely be assigned as $TO_{\text{Cd-Se}}$. This solves the raised issue at the beginning of the section.

In Fig. 9, the relevant θ angle per spectrum is estimated from a careful contour modeling (paying attention to both the Raman intensity and the Raman frequency) of the PP band using the generic RCS(ω, y) formula given in Ref. 47. y is expressed in its θ-dependence via the wavevector conservation law. The procedure is detailed as Fig. S3 in the supplementary material.

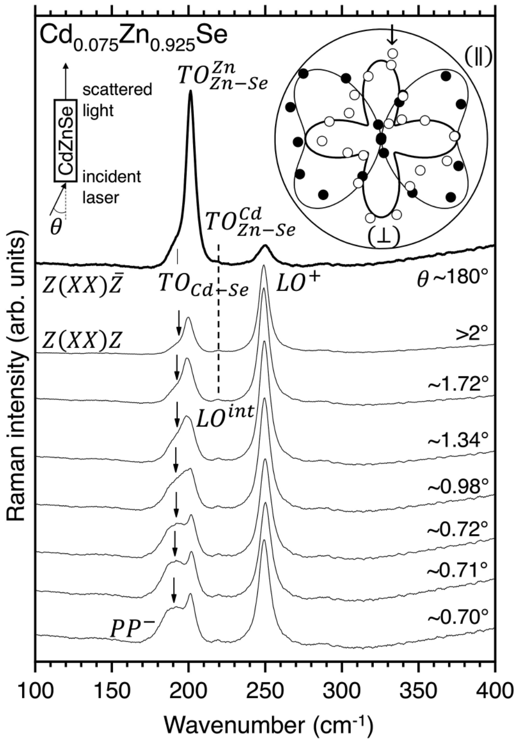

FIG. 9. $Cd_{0.075}Zn_{0.925}$Se-c near-forward PP Raman spectra. Cross-polarized near-forward $Cd_{0.075}Zn_{0.925}$Se-c Raman spectra taken with the 514.5 nm laser line at various small scattering angles (θ) onto a (110)-cleaved face. The backscattering Raman at a large scattering angle is added (upper curve) for reference purpose. Inset: symmetry analysis of the strong PP^{-} band at a minimal scattering angle θ using crossed (⊥, open symbols) and parallel (∥, full symbols) polarizations (inset). The theoretical Greek crosslike (⊥, thick curve) and butterflylike (∥, thin curve) patterns are shown for reference purpose. The Raman intensities (normalized to the maximum value in each series) match over a complete revolution (360°) of the (⊥,∥)-polarization pairs at the sample surface (see the arrow).

C. Upper-minor TO^{Cd}_{Zn-Se} mode: κ-equipped version of the percolation scheme

The only remaining issues relate to the upper/minor in-band (LO^{int}, $TO^{Cd}_{Zn\text{-}Se}$) mode. The latter is theoretically LO–TO inverted beyond experimental resolution (at least in the case of $Cd_{0.170}Zn_{0.830}$Se-c, see Fig. 1). In fact, the TO and LO components of the in-band mode appear to be degenerate in our raw Raman data (dashed-dotted lines in Fig. 7) and also in the IR[28] ones. This goes with another disconcerting feature that the in-band ($TO^{Cd}_{Zn\text{-}Se}$) mode is hardly detected in our pure-TO Raman spectra (Fig. 7). Satisfactory agreement between the theoretical [two curves, the inset of Fig. 7(b)] and experimental [bottom curve, Fig. 7(b)] $Cd_{0.170}Zn_{0.830}$Se-c Raman lineshapes can be achieved only if the oscillator strength awarded to the upper/in-band mode is roughly divided by two [lower curve, the inset of Fig. 7(b)] with respect to its nominal value fixed by the f-terms in Fig. 1 [upper curve, the inset of Fig. 7(b)]. The combined (LO–TO) frequency and (TO) intensity anomalies affecting the same (upper/in-band) Raman mode cannot be merely fortuitous, suggesting a common origin.

An option is a deviation from the ideal random Zn ↔ Cd substitution toward local clustering. This means that the Zn-Se bonds "prefer" to vibrate in their (ZnSe-like) environment rather than in the foreign (CdSe-like) one. In this case, the (lower) $TO^{Zn}_{Zn\text{-}Se}$ mode becomes over-represented at the expense of the (upper) $TO^{Cd}_{Zn\text{-}Se}$ one [emphasized by opposite arrows in the inset of Fig. 7(b)]. Indeed, any $TO^{Cd}_{Zn\text{-}Se} \rightarrow TO^{Zn}_{Zn\text{-}Se}$ transfer of oscillator strength would dramatically reduce both the TO Raman intensity and the TO–LO splitting (whether inverted or not) of the "supplier" mode (to the benefit of the "recipient" one).

Such an option is independently supported by an experimental observation done by Kozyrev that the $TO^{Zn}_{Zn\text{-}Se}$ and $TO^{Cd}_{Zn\text{-}Se}$ IR-features due to Cd_xZn_{1-x}Se-c single crystals are over-represented and subrepresented in comparison with their counterparts stemming from epitaxial layers (Sec. I—see Fig. 2 of Ref. 29), respectively. This provides a direct experimental evidence for an effective transfer of oscillator strength between the two modes. Furthermore, it relates the transfer in question to the crystal-growth conditions, which, in turn, ultimately govern the nature of the atom substitution.[45] Besides, Brafman[19] has indicated a trend toward Zn and Cd separation (clustering) in his zincblende-type single crystals. In this case, the separation occurs in the form of a superlattice-type alternating pattern of ZnSe-rich and CdSe-rich series of high-density (111)-stacking planes of the zincblende structure. In his case, such long-range ordering was needed to explain the anisotropy of the considered crystal under a polarizing microscope and by X-ray diffraction. In our case, no extinction is observed with our zincblende-type single crystals under a polarizing microscope. This means that the long-range ordering is excluded, independently confirmed by X-ray diffraction (Sec. II A). Still, Brafman's and Kozyrev's observations converge to state that the zincblende-type Cd_xZn_{1-x}Se-c single crystals are prone to clustering. The next issue is to estimate the amount of clustering in the current Cd_xZn_{1-x}Se-c samples.

1. κ-dependent 1D-oscillator fractions

The trend toward local clustering can be formalized within the percolation scheme by expressing the individual fractions of 1D-oscillators behind the three {$TO_{Cd\text{-}Se}$, $TO^{Zn}_{Zn\text{-}Se}$, $TO^{Cd}_{Zn\text{-}Se}$} modes of Cd_xZn_{1-x}Se in their dependence on a relevant order parameter κ. We basically proceed along the approach developed by Verleur and Barker in their cluster model[66]—as was done in working out the κ-dependent version of the percolation scheme for the Ge_xSi_{1-x} mixed crystal with diamond structure.[65,75] However, care is taken that our percolation-type oscillators are defined at the second-neighbor scale at one dimension (1D), whereas the Se-centered cluster units of the cluster model refer to the first-neighbor scale in the real three-dimensional (3D) crystal.

An order parameter κ operating at the first-neighbor scale for Zn is introduced via the probability P_{ZnZn} for a given site next to a substituent site occupied by Zn to be also occupied by Zn, according to

$$P_{ZnZn}(x,\kappa) = P_{Zn}(x) + \kappa P_{Cd}(x) = (1-x) + \kappa x.$$

A similar order parameter κ' for Cd is used to express P_{CdCd} as

$$P_{\mathrm{CdCd}}(x, \kappa) = P_{\mathrm{Cd}}(x) + \kappa' P_{\mathrm{Zn}}(x) = x + \kappa'(1 - x).$$

In the above expressions, $P_X(x)$ is the probability for a given substituent site to be occupied by X standing for Zn or Cd, namely, $(1 - x)$ or x, respectively. The probability to form a ZnCd pair on the substituent 1D-sublattice can be written as $P_{\mathrm{ZnCd}}(x, \kappa)$ or $P_{\mathrm{CdZn}}(x, \kappa)$, leading to $\kappa = \kappa'$.

Alternative order parameters κ_1 and κ_2 can likewise be defined for Zn and Cd at the second-neighbor scale, according to

$$P_{\mathrm{ZnZnZn}}(x, \kappa) = P_{\mathrm{Zn}}(x) P_{\mathrm{ZnZn}}(x) P_{\mathrm{ZnZnZn}}(x) = (1 - x) + \kappa_1 x,$$

$$P_{\mathrm{CdCdCd}}(x, \kappa) = x + \kappa_2(1 - x).$$

The probabilities to form the ZnCdCd and ZnZnCd triplets are the same whether starting or ending by Zn. Considering further that the alternate occupancy by Zn and Cd of the starting sites of a triplet cancels a trend toward local clustering—meaning that $P_{\mathrm{CdZnX}} = P_X$ for any X, and also that $P_{\mathrm{ZnCd}} = 1 - P_{\mathrm{ZnZn}}$ (and $P_{\mathrm{CdZn}} = 1 - P_{\mathrm{CdCd}}$), one arrives at $\kappa_1 = \kappa P^{-1}_{\mathrm{ZnZn}}(x, \kappa)$ and $\kappa_2 = \kappa P^{-1}_{\mathrm{CdCd}}(x, \kappa)$. With this, all probabilities become κ-dependent.

As already mentioned, the Cd-Se vibration ($TO_{\mathrm{Cd\text{-}Se}}$) is blind to its local environment. In contrast, the Zn-Se one distinguishes between all-Cd ($TO^{\mathrm{Cd}}_{\mathrm{Zn\text{-}Se}}$) and all-remaining ($TO^{\mathrm{Zn}}_{\mathrm{Zn\text{-}Se}}$) environments at the second-neighbor scale (Sec. III)—including all-Zn ones together with all possible variants in (Zn,Cd)-mixed ones. Accordingly, the κ-dependent fractions of 1D-oscillators behind such modes are expressed as

$$\begin{aligned} f_{\mathrm{Cd\text{-}Se}}(x, \kappa) &= x, \\ f^{\mathrm{Zn}}_{\mathrm{Zn\text{-}Se}}(x, \kappa) &= (1 - x)\{P_{\mathrm{ZnZn}} P_{\mathrm{ZnZnZn}} + 2x(1 - P_{\mathrm{CdCd}})\}, \\ f^{\mathrm{Cd}}_{\mathrm{Zn\text{-}Se}}(x, \kappa) &= x^2(1 - P_{\mathrm{CdCd}}). \end{aligned}$$

respectively. The (x, κ)-dependence of the pair- and triplet-related probabilities is omitted for clarity. A basic conservation rule concerned with the κ-independent fraction of Zn atoms in the crystal leads to $f^{\mathrm{Zn}}_{\mathrm{Zn\text{-}Se}}(x, \kappa) + f^{\mathrm{Cd}}_{\mathrm{Zn\text{-}Se}}(x, \kappa) = (1 - x)$.

The random Zn ↔ Cd substitution is achieved at $\kappa = 0$. In this case, the above $f(x, \kappa)$-terms match the $f(x)$-terms given in Fig. 1. Positive and negative κ values reflect trends toward local clustering and local anticlustering, respectively. In particular, $\kappa = 1$ refers to full clustering, i.e., to the actual phase separation at the local scale. The full anticlustering, corresponding to $\kappa = -1$, can fully develop only at $x = 0.5$, being clear that outside $x = 0.5$, some at least of the dominant substituents have first-neighbors of the like species. The minimal κ value at a given composition x is achieved when the minor 1D-oscillator defined at the nearest-neighbor scale (for simplicity) disappears, leading to

$$\kappa_{\min} = \max\left\{-\frac{x}{1 - x}, -\frac{1 - x}{x}\right\}.$$

A more refined estimate can be obtained for local environments defined at the second-neighbor scale, as in the present case. However, the above $\kappa_{\min}$ value is sufficient to fix ideas, especially since, apparently, $\mathrm{Cd}_x\mathrm{Zn}_{1-x}\mathrm{Se}$ is not prone to anticlustering (see below).

2. $\mathrm{Cd}_x\mathrm{Zn}_{1-x}\mathrm{Se}$ Raman spectra in their κ-dependence

The (x, κ)-dependent 1D-oscillator fractions (f-terms above) govern both the oscillator strength and Faust-Henry coefficients awarded per $\{TO_{\mathrm{Cd\text{-}Se}}, TO^{\mathrm{Zn}}_{\mathrm{Zn\text{-}Se}}, TO^{\mathrm{Cd}}_{\mathrm{Zn\text{-}Se}}\}$ mode in the generic multimode RCS formula (Sec. IV B). The κ value required to mimic the apparent collapse of the $TO^{\mathrm{Cd}}_{\mathrm{Zn\text{-}Se}}$ intensity of $\mathrm{Cd}_{0.170}\mathrm{Zn}_{0.830}\mathrm{Se}$-c by roughly half the reference value for the random ($\kappa = 0$) crystal (Sec. IV C)—to the benefit of $TO^{\mathrm{Zn}}_{\mathrm{Zn\text{-}Se}}$ [refer to the antagonist arrows in the inset of Fig. 7(b)]—amounts to ∼0.5. At such κ value, the inverted $LO^{int} - TO^{\mathrm{Cd}}_{\mathrm{Zn\text{-}Se}}$ splitting almost vanishes below the experimental detection limit (Fig. 1), consistently with experimental findings (Fig. 7, dashed-dotted lines). Incidentally, the C_{FH} value of CdSe-c, i.e., −0.99 (Sec. II B), was adjusted at this occasion, i.e., so as to best mimic the experimental $TO_{\mathrm{Cd\text{-}Se}}/TO^{\mathrm{Zn}}_{\mathrm{Zn\text{-}Se}}$ intensity ratio at the retained κ value.

A direct evidence that the $TO^{\mathrm{Zn}}_{\mathrm{Zn\text{-}Se}} \leftarrow TO^{\mathrm{Cd}}_{\mathrm{Zn\text{-}Se}}$ transfer of oscillator strength behind the $LO^{+} - TO^{\mathrm{Cd}}_{\mathrm{Zn\text{-}Se}}$ degeneracy apparent in the Raman/IR spectra is actually due to clustering is searched by comparing in Fig. 10(a) the *ab initio* (AIMPRO) Raman spectra of two 216-atom $\mathrm{Cd}_{0.3}\mathrm{Zn}_{0.7}\mathrm{Se}$ supercells, i.e., a random one ($\kappa = 0$; solid line) and a clustered one corresponding to the maximum achievable κ value of 0.4 (dashed curve)—see Sec. II C. The *ab initio* study is placed at $x \sim 0.3$ because the CdSe- and ZnSe-like environments (of the percolation scheme) are both well represented at this composition, while keeping a proximity with the studied Cd contents in this work. This composition is furthermore symbolic as it coincides with the zincblende ↔ wurtzite structural transition (Sec. I). The corresponding $\mathrm{Im}\{\varepsilon_r(\omega, x = 0.3)\}$ curve constructed by Kozyrev from his IR-data (digitized from Fig. 1 of Ref. 18) is added for reference purpose. When shifting from the random ($\kappa = 0$) supercell to the clustered ($\kappa = 0.4$) one, antagonist variations of the lower-$TO^{\mathrm{Zn}}_{\mathrm{Zn\text{-}Se}}$ (turned off) and upper-$TO^{\mathrm{Cd}}_{\mathrm{Zn\text{-}Se}}$ (magnified) *ab initio* Raman features [curved arrow in relation to the shaded areas in Fig. 10(a)] reveal an actual transfer of oscillator strength. The *ab initio* test is thus conclusive in the positive sense.

The microstructures of both supercells are shown in Figs. 10(b) ($\kappa = 0$) and 10(c) ($\kappa = 0.4$). In each case, the (invariant) Se atoms are distinguished (using a color code) depending on their five possible tetrahedral (Cd,Zn)-first-neighbor environments (from all-Zn to all-Cd). The substituent (Zn,Cd)-sublattice is removed for clarity. The basic trend with clustering ($\kappa > 0$) is that the homo (pure-Zn and pure-Cd) Se-units are favored at the expense of the hetero (Zn/Cd-mixed) ones with respect to the random case ($\kappa = 0$). A more statistical insight obtained by comparing the κ-dependent binomial Bernoulli distributions of the Se-centered units in the random ($\kappa = 0$) and clustered ($\kappa = 0.5$) cases using the formulas given in Ref. 66 is reported as Fig. S4 in the supplementary material.

To our view, the trend toward local clustering of the $\mathrm{Cd}_x\mathrm{Zn}_{1-x}\mathrm{Se}$-c single crystals may not relate to the large lattice mismatch (∼7%). Indeed, the latter is larger in $\mathrm{Zn}_{1-x}\mathrm{Be}_x\mathrm{Se}$-c (∼9%), further aggravated by a dramatic contrast in bond stiffness,[11,70] and, still, random $\mathrm{Zn}_{1-x}\mathrm{Be}_x\mathrm{Se}$-c single crystals can be grown throughout the composition domain.[76] The local clustering

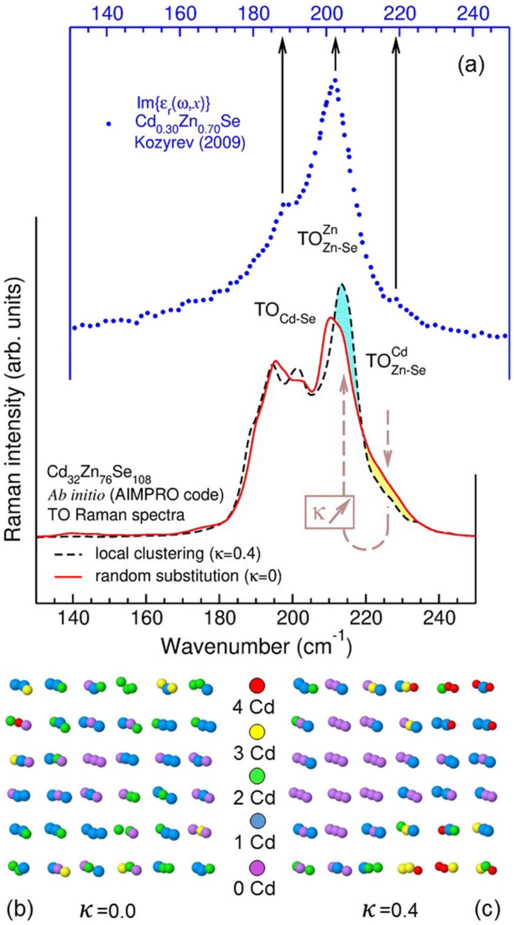

FIG. 10. $Cd_{0.3}Zn_{0.7}Se$-c *ab initio* Raman spectra. (a) *Ab initio* TO Raman spectra obtained by applying the AIMPRO code to random ($\kappa = 0$, continuous line) and clustered ($\kappa = 0.4$, dashed line) $Cd_{32}Zn_{76}Se_{108}$ cubic supercells. The corresponding $\mathrm{Im}\{\varepsilon_r(\omega, x = 0.30)\}$ spectrum (shifted horizontally) reconstructed from IR-reflectivity data (Ref. 18) is shown (dotted line) for comparison. The Se atoms in the random (b) and clustered (c) supercells are distinguished depending on their local environment at the first-neighbor scale, as schematically indicated.

apparent in $Cd_xZn_{1-x}Se$-c would rather reflect a microstructural instability on approach to the composition-induced zincblende ↔ wurtzite structural transition ($x \sim 0.3$). If we refer to the IR data reported by Kozyrev (Fig. 2 from Ref. 29, reproduced as Fig. S4 in the supplementary material), this instability freely develops in the single crystals grown under equilibrium conditions, whereas it is frustrated in the thin films grown out of equilibrium conditions.

V. CONCLUSION

We report a pure-TO Raman study of zincblende-type $Cd_xZn_{1-x}Se$ single crystals ($x \leq 0.3$). Both the phonon-polariton regime, so far unexplored in this system, and the native purely-mechanical phonon regime behind the phonon-polaritons are addressed using suitable near-forward and backward Raman scattering geometries implemented onto (110)-oriented faces obtained by cleavage, respectively. The discussion of the Raman data is supported by *ab initio* calculations done in the purely-mechanical TO-phonon regime, with a double input. First, *ab initio* calculations done with the Siesta code, concerned with the Γ-PhDOS of prototype impurity motifs ($x \sim 0, 1$) at sensitive TO Raman frequencies, help to assign the Raman modes *de visu* based on the examination of the actual vibration patterns. Second, *ab initio* Raman spectra obtained by applying the AIMPRO code to large supercells (∼200 atoms) provide decisive insights into the TO Raman intensities ($x \sim 0.3$ and $x \sim 0.5$). This is needed, in particular, to elucidate the sensitivity of the Zn-Se vibration to its local environment, eventually found to operate at the second-neighbor scale. We conclude to a three-mode $\{TO_{\text{Cd-Se}}, TO^{\text{Zn}}_{\text{Zn-Se}}, TO^{\text{Cd}}_{\text{Zn-Se}}\}$ percolation-type Raman/IR pattern for $Cd_xZn_{1-x}Se$, as anticipated by Kozyrev based on his careful IR study.[29]

Apparent anomalies concerned with the quasinegligible LO–TO inversion of the upper/minor in-band mode and with the surprisingly small Raman intensity of its TO component find a natural explanation by considering a clear deviation from the ideal Zn ↔ Cd random substitution toward local clustering. This reflects a microstructural instability on approach to the composition-induced zincblende ↔ wurtzite structural transition (x∼0.3). The amount of clustering is estimated by adapting to the zincblende structure a version of the percolation model equipped with a relevant order parameter κ, in the same spirit as earlier done for the Ge_xSi_{1-x} mixed crystal with diamond structure.[65,75] The AIMPRO *ab initio* calculations provide a decisive support with this respect by tracing the Raman intensities in their dependence on local clustering.

Generally, this work illustrates how the nominal Raman signal of common semiconductor mixed crystals with zincblende structures can be exploited within the percolation scheme to diagnose and estimate (in a straightforward and nondestructive manner) any deviation from the ideal random substitution—the central issue when dealing with mixed crystals (see, e.g., Refs. 45 and 77). Such insight was not possible with the traditional models, i.e., neither with the MREI one (by construction) nor with the cluster one (due to a conceptual bias), as discussed, e.g., in Ref. 75. With this respect, the percolation scheme fills a gap.

SUPPLEMENTARY MATERIAL

See the supplementary material concerning (i) the formalization of the phonon-mode behavior of the $Cd_xZn_{1-x}Se$ mixed crystal within the percolation scheme, (ii) additional polarized Raman data, and (iii) statistical aspects related to clustering in this system, notably in relation to the current *ab initio* calculations.

ACKNOWLEDGMENTS

We acknowledge assistance from the Psiché beamline staff of synchrotron SOLEIL for the X-ray diffraction measurements and from the Ellipsometry core facility of LCP-A2MC (Université de Lorraine—http://lcp-a2mc.univ-lorraine.fr). We thank L. Johann and P. Franchetti for technical assistance in the ellipsometry and Raman measurements, respectively. This work was funded by FEDER funds through the COMPETE 2020 Programme and

National Funds through FCT—Portuguese Foundation for Science and Technology under Project No. UID/CTM/50025/2019.

REFERENCES

[1] S. Adachi and T. Taguchi, Phys. Rev. B **43**, 9569 (1991).

[2] S. Niromiya and S. Adachi, J. Appl. Phys. **78**, 4681 (1995).

[3] K. Suzuki and S. Adachi, J. Appl. Phys. **83**, 1018 (1998).

[4] S. Y. Wang, Y. Kawakami, J. Simpson, H. Stewart, K. A. Prior, and B. C. Cavenett, Appl. Phys. Lett. **62**, 1715 (1993).

[5] Y. D. Kim, M. V. Klein, S. F. Ren, Y. C. Chang, H. Luo, N. Samarth, and J. K. Furdyna, Phys. Rev. B **49**, 7262 (1994).

[6] C. Jordan, J. F. Donegan, J. Hegarty, B. J. Roycroft, S. Taniguchi, T. Hino, E. Kato, N. Noguchi, and A. Ishibashi, Appl. Phys. Lett. **74**, 3359 (1999).

[7] N. Samarth, H. Luo, J. K. Furdyna, R. G. Alonso, Y. R. Lee, A. K. Ramdas, S. B. Qadri, and N. Otsuka, Appl. Phys. Lett. **56**, 1163 (1990).

[8] Z. H. Huang, S. D. Liang, C. Y. Chen, and D. L. Lin, Solid State Commun. **104**, 281 (1997).

[9] Z. Z. Guo, X. X. Liang, and S. L. Ban, Phys. Status Solidi B **238**, 173 (2003).

[10] P. Y. Yu and M. Cardona, *Fundamentals of Semiconductors*, 4th ed. (Springer-Verlag, Heidelberg, 2010), Chap. 3, pp. 107–158.

[11] N. E. Christensen, S. Satpathy, and Z. Pawlowska, Phys. Rev. B **36**, 1032 (1987).

[12] A. S. Nasibov, Y. V. Korostelin, P. V. Shapkin, L. G. Suslina, D. L. Fedorov, and L. S. Markov, Solid State Commun. **71**, 867 (1989).

[13] S. P. Kozyrev, Phys. Solid State **51**, 1004 (2009).

[14] B. Hennion, F. Moussa, G. Pepy, and K. Kunc, Phys. Lett. A **36**, 376 (1971).

[15] Z. Tian, M. Li, Z. Ren, H. Ma, A. Alatas, S. D. Wilson, and J. Li, J. Phys. Condens. Matter **27**, 375403 (2015).

[16] W. S. Li, Z. X. Shen, D. Z. Shen, and X. W. Fan, J. Appl. Phys. **84**, 5198 (1998).

[17] W. Meredith, G. Horsburgh, G. D. Brownlie, K. A. Prior, B. C. Cavenett, W. Rothwell, and A. J. Dann, J. Cryst. Growth **159**, 103 (1996).

[18] S. P. Kozyrev, Phys. Solid State **50**, 1117 (2008).

[19] O. Brafman, Solid State Commun. **11**, 447 (1972).

[20] I. F. Chang and S. S. Mitra, Phys. Rev. **172**, 924 (1968).

[21] M. Y. Valakh, M. P. Lisitsa, V. I. Sidorenko, and G. N. Polissky, Phys. Lett. **78**, 115 (1980).

[22] M. Y. Valakh, A. P. Litvinchuck, G. S. Pekar, and G. N. Polysskii, Phys. Status Solidi B **104**, 743 (1981).

[23] M. Y. Valakh, M. P. Lisitsa, G. S. Pekar, G. N. Polysskii, V. I. Sidorenko, and A. M. Yaremko, Phys. Status Solidi B **113**, 635 (1982).

[24] R. G. Alonso, E.-K. Suh, A. K. Ramdas, N. Samarth, H. Luo, and J. K. Furdyna, Phys. Rev. B **40**, 3720 (1989).

[25] J. Avendaño-López, F. L. Castillo-Alvarado, A. Escamilla-Esquivel, G. Contreras-Puente, J. Ortiz-López, and O. Zelaya-Angel, Solid State Commun. **100**, 33 (1996).

[26] L. K. Vodop'yanov, S. P. Kozyrev, and Y. G. Sadof'ev, Phys. Solid State **41**, 893 (1999).

[27] E. A. Vinogradov, B. N. Mavrin, and L. K. Vodop'yanov, J. Exp. Theor. Phys. **99**, 749 (2004).

[28] L. K. Vodopyanov, E. A. Vinogradov, V. S. Vinogradov, I. V. Kucherenko, B. N. Mavrin, N. N. Novikova, and P. V. Shapkin, Phys. Status Solidi C **1**, 3162 (2004).

[29] S. P. Kozyrev, Semiconductors **48**, 1261 (2014).

[30] O. Pagès, A. V. Postnikov, M. Kassem, A. Chafi, A. Nassour, and S. Doyen, Phys. Rev. B **77**, 125208 (2008).

[31] S. Eckner, K. Ritter, P. Schöppe, E. Haubold, E. Eckner, J. Rensberg, R. Röder, M. C. Ridgway, and C. S. Schnohr, Phys. Rev. B **97**, 195202 (2018).

[32] S. Eckner, A. Johannes, M. Gnauck, H. Kämmer, T. Steinbach, S. Schönherr, R. Chernikov, E. Welter, M. C. Ridgway, and C. S. Schnohr, Europhys. Lett. **126**, 36002 (2019).

[33] D. W. Taylor, *Optical Properties of Mixed Crystals*, edited by R. J. Elliott and I. P. Ipatova (Elsevier Science Publishers B.V., 1988), Chap. 2, p. 35 (cf. Table 3, p. 78).

[34] S. Adachi, *Properties of Semiconductor Alloys: Group-IV, III-V and II-VI Semiconductors* (John Wiley & Sons, Inc., Chichester, 2009), Chap. 4, p. 100.

[35] E. Jahne, Phys. Status Solidi B **74**, 275 (1976).

[36] E. Jahne, Phys. Status Solidi B **75**, 221 (1976).

[37] O. Pagès, M. Ajjoun, T. Tite, D. Bormann, E. Tournié, and K. C. Rustagi, Phys. Rev. B **70**, 155319 (2004).

[38] R. Hajj Hussein, O. Pagès, S. Doyen-Schuler, H. Dicko, A. V. Postnikov, F. Firszt, A. Marasek, W. Paszkowicz, A. Maillard, L. Broch, and O. Gorochov, J. Alloys Compd. **644**, 704 (2015).

[39] J. M. Soler, E. Artacho, J. D. Gale, A. García, J. Junquera, P. Ordejón, and D. Sánchez-Portal, J. Phys. Condens. Matter **14**, 2745 (2002).

[40] R. Jones and P. R. Briddon, "Semiconductors and semimetals," in Identification of Defects in Semiconductors (Academic Press, Boston, 1988), Vol. 51A, Chap. 6.

[41] P. R. Briddon and R. Jones, Phys. Status Solidi B **217**, 131 (2000).

[42] M. J. Rayson and P. R. Briddon, Comput. Phys. Commun. **178**, 128 (2008).

[43] F. Firszt, A. A. Wronkowska, A. Wronkowski, S. Łęgowski, A. Marasek, H. Męczyńska, M. Pawlak, W. Paszkowicz, K. Strzałkowski, and A. J. Zakrzewski, Cryst. Res. Technol. **40**, 386 (2005).

[44] F. C. Peiris, S. Lee, U. Bindley, and J. K. Furdyna, J. Appl. Phys. **86**, 918 (1999).

[45] A. Mascarenhas, *Spontaneous Ordering in Semiconductor Alloys* (Kluwer Academic, Plenum Publishers, New York, 2002).

[46] J. Geurts, Surf. Sci. Rep. **18**, 1 (1993).

[47] H. Dicko, O. Pagès, F. Firszt, K. Strałkowski, A. Maillard, C. Jobard, and L. Broch, J. Appl. Phys. **120**, 185702 (2016).

[48] C. A. Arguello, D. L. Rousseau, and S. P. S. Porto, Phys. Rev. **181**, 1351 (1969).

[49] J. Groenen, R. Carles, G. Landa, C. Guerret-Piécourt, C. Fontaine, and M. Gendry, Phys. Rev. B **58**, 10452 (1998).

[50] M. Cardona, *Light Scattering in Solids II*, Topics in Applied Physics Vol. 50, edited by M. Cardona and G. Günterodt (Springer, Berlin, 1982), Chap. 2, p. 62.

[51] R. Cuscó, V. Consonni, E. Bellet-Amalric, R. André, and L. Artús, Phys. Status Solidi Rapid Res. Lett. **11**, 1700006 (2017).

[52] N. Troullier and J. L. Martins, Phys. Rev. B **43**, 1993 (1991).

[53] J. P. Perdew and Y. Wang, Phys. Rev. B **45**, 13244 (1992).

[54] C. Hartwigsen, S. Goedecker, and J. Hutter, Phys. Rev. B **58**, 3641 (1998).

[55] H. J. Monkhorst and J. D. Pack, Phys. Rev. B **13**, 5188 (1976).

[56] F. Birch, Phys. Rev. **71**, 809 (1947).

[57] B. Jobst, D. Hommel, U. Lunz, T. Gerhard, and G. Landwehr, Appl. Phys. Lett. **69**, 97 (1996).

[58] S. Ves, K. Strössner, N. E. Christensen, C. K. Kim, and M. Cardona, Solid State Commun. **56**, 479 (1985).

[59] S. Baroni, S. de Gironcoli, and P. Giannozzi, Phys. Rev. Lett. **65**, 84 (1990).

[60] *Landolt-Börnstein: Numerical Data and Functional Relationships in Science and Technology*, edited by O. Madelung, M. Schulz, and H. Weiss (Springer, Berlin, 1982), Vol. 17.

[61] S. de Gironcoli, Phys. Rev. B **46**, 2412 (1992).

[62] Y.-S. Lim, S.-C. Yoon, K.-J. Yee, Y.-H. Ahn, E. Oh, and J.-H. Lee, Appl. Phys. Lett. **82**, 2446 (2003).

[63] E. Deligoz, K. Colakoglu, and Y. Ciftci, Physica B **373**, 124 (2006).

[64] S. Kirkpatrick, C. D. Gelatt, Jr., and M. P. Vecchi, Science **220**, 671 (1983).

[65] V. J. B. Torres, R. Hajj Hussein, O. Pagès, and M. J. Rayson, J. Appl. Phys. **121**, 085704 (2017).

[66] H. W. Verleur and A. S. Barker, Jr., Phys. Rev. **149**, 715 (1966).

[67] A. Zunger, S.-H. Wei, L. G. Ferreira, and J. E. Bernard, Phys. Rev. Lett. **65**, 353 (1990).

[68] S. H. Wei, L. G. Ferreira, J. E. Bernard, and A. Zunger, Phys. Rev. B **42**, 9622 (1990).

[69] B. D. Rajput and D. A. Browne, Phys. Rev. B **53**, 9052 (1996).
[70] C. Vèrié, J. Cryst. Growth **184/185**, 1061 (1998).
[71] H. Dicko, O. Pagès, R. Hajj Hussein, G. K. Pradhan, C. Narayana, F. Firszt, A. Marasek, W. Paszkowicz, A. Maillard, C. Jobard, L. Broch, and F. El Hajj Hassan, J. Raman Spectrosc. **47**, 357 (2016).
[72] H. Dicko, O. Pagès, M. B. Shoker, F. Firszt, K. Strzałkowski, A. Maillard, A. Polian, Y. Battie, L. Broch, A. En Naciri, A. V. Postnikov, W. Paszkowicz, and J.-P. Itié, Sci. Rep. **9**, 7817 (2019).
[73] Independently achievable by solving numerically the characteristic dispersion of a TO mode, i.e., $\varepsilon_r(\omega, x) = \binom{q\cdot c}{\omega}^2$.
[74] C. H. Henry and J. J. Hopfield, Phys. Rev. Lett. **15**, 964 (1965).
[75] O. Pagès, R. Hajj Hussein, and V. J. B. Torres, J. Appl. Phys. **114**, 033513 (2013).
[76] O. Pagès, A. V. Postnikov, A. Chafi, D. Bormann, P. Simon, F. Glas, F. Firszt, W. Paszkowicz, and E. Tournié, Eur. Phys. J. B **73**, 461 (2010).
[77] L. Bellaiche and A. Zunger, Phys. Rev. B **57**, 4425 (1998).